

Review Article

Femtoscopic and Nonfemtoscopic Two-Particle Correlations in $A + A$ and $p + p$ Collisions at RHIC and LHC Energies

Yu. M. Sinyukov,¹ S. V. Akkelin,¹ Iu. A. Karpenko,^{1,2} and V. M. Shapoval¹

¹ Bogolyubov Institute for Theoretical Physics, Kiev 03680, Ukraine

² FIAS, 60438 Frankfurt am Main, Germany

Correspondence should be addressed to Yu. M. Sinyukov; sinyukov@bitp.kiev.ua

Received 15 April 2013; Accepted 16 June 2013

Academic Editor: Edward Sarkisyan-Grinbaum

Copyright © 2013 Yu. M. Sinyukov et al. This is an open access article distributed under the Creative Commons Attribution License, which permits unrestricted use, distribution, and reproduction in any medium, provided the original work is properly cited.

The theoretical review of the last femtoscopy results for the systems created in ultrarelativistic $A + A$, $p + p$, and $p + Pb$ collisions is presented. The basic model, allowing to describe the interferometry data at SPS, RHIC, and LHC, is the hydrokinetic model. The model allows one to avoid the principal problem of the particlization of the medium at nonspace-like sites of transition hypersurfaces and switch to hadronic cascade at a space-like hypersurface with nonequibrated particle input. The results for pion and kaon interferometry scales in $Pb + Pb$ and $Au + Au$ collisions at LHC and RHIC are presented for different centralities. The new theoretical results as for the femtoscopy of small sources with sizes of 1-2 fm or less are discussed. The uncertainty principle destroys the standard approach of completely chaotic sources: the emitters in such sources cannot radiate independently and incoherently. As a result, the observed femtoscopy scales are reduced, and the Bose-Einstein correlation function is suppressed. The results are applied for the femtoscopy analysis of $p + p$ collisions at $\sqrt{s} = 7$ TeV LHC energy and $p + Pb$ ones at $\sqrt{s} = 5.02$ TeV. The behavior of the corresponding interferometry volumes on multiplicity is compared with what is happening for central $A + A$ collisions. In addition the nonfemtoscopic two-pion correlations in proton-proton collisions at the LHC energies are considered, and a simple model that takes into account correlations induced by the conservation laws and minijets is analyzed.

1. Introduction

The two-particle correlation femtoscopy of identical particles allows one to analyze the space-time structure of a particle emission from the systems created in heavy ion, hadron and lepton collisions (for recent reviews see, e.g., [1–3]). The femtoscopy method, which is based on the Bose-Einstein or Fermi-Dirac interference of identical particles, has been proposed first in [4–7] for measurements of the geometrical sizes and shapes of the interaction region in hadronic collisions. Then it has been developed in [8–14] as a tool for a study of rapidly expanding fireballs formed in ultrarelativistic heavy ion collisions. Despite the extremely small sizes of such systems (the order of the value is around 10^{-14} m), they have a pronounced inhomogeneous structure. The generalized treatment of the interferometry measurements asserts that the measured scales—the interferometry radii—are associated just with the homogeneity lengths in the system [15–18]. Only in the very particular case of a

finite homogeneous system such lengths correspond to the total geometrical sizes, but normally they are smaller than the latter. The interferometry scanning of femtosystems at various total momenta of pion pairs allows one to analyze the homogeneity lengths related to different space-time regions of the expanding fireball [11, 12, 17, 18]. An understanding of interferometry in terms of the homogeneity lengths, as opposed to the simple-mind geometrical picture, provides explanation to some, at first sight paradoxical, results at RHIC.

The long-term study of the peculiarities of the interferometry scales behavior in heavy ion collisions, in particular, the so-called RHIC HBT puzzle [19–21], relatively small observed radii and close to unity ratio of the two transverse femtoscales, helps much in clearing up the underlying properties of the matter created in these processes. The physical conditions explaining the RHIC HBT puzzle are [22–28] a relatively hard EoS because of a crossover transition (instead of the 1st order one) between quark-gluon and hadron

phases, the presence of prethermal anisotropic transverse flow developed to thermalization time, and an “additional portion” of the transverse flow caused by the shear viscosity effect and fluctuations of the initial conditions. An account for these factors gives the possibility to describe well the hadron spectra together with the femtoscopy data within a realistic freeze-out hydrokinetic model (HKM) with a gradual decay of the fluid into observed particles [28–30].

Soon after the first Large Hadron Collider (LHC) heavy ion results were received, it became evident that the hydrodynamic picture of the collision processes, confirmed at RHIC, is clearly seen also at much higher energy. This conclusion is based on the two classes of observables. The first one is related to the azimuthal anisotropy of particle spectra expressed basically through their second harmonics or v_2 coefficients. The obtained LHC results for the transverse momentum dependence of $v_2(p_T)$ at a given centrality bin (here and below for the quantities depending on one particle momentum p_T means the transverse momentum of one particle, whereas for the pair quantities p_T means the average pair transverse momentum, $p_T = (p_{1T} + p_{2T})/2$) were found to be similar to the ones at RHIC, except for the higher momentum range at LHC [31]. This is the evidence of the same hydrodynamic mechanism of the anisotropy formation as at RHIC. The second type of observables deals with the direct measurements of the space-time structure of nucleus-nucleus collisions by means of the correlation femtoscopy. The hydrodynamic predictions [32] for p_T behavior of the interferometry radii at the LHC energies were confirmed by the ALICE experiment [33]. The most impressive hydrodynamic prediction [28, 34], that the ratio of the two transverse interferometry radii, *out* to *side*, will drop in the whole p_T -interval with increasing collision energy and will reach a value close to unity at the LHC, has been discovered experimentally [33].

However, quantitative application of the hydrodynamic approach is a nontrivial problem, because it depends on both the initial conditions for the continuous matter evolution and final state treatments for the particles production. The hydrokinetic model (HKM) [23, 29, 35] allows one to apply hydrodynamics also at the late nonequilibrated stage of gradual system decay, where it can be matched, in its hybrid version (hHKM) [30, 36], with the ultrarelativistic quantum molecular dynamics (UrQMD) cascade [37, 38]. A utilization of the UrQMD ensures an adequate description of the very rarefied stage of matter evolution and transition to particle free-streaming regime. It is especially important at the LHC energies because of relatively prolonged duration of the interacting nonequilibrated stage. It was shown that the hydrokinetic approach without such correction of later-time evolution results in overestimated effective temperature of proton spectra at RHIC energy and insufficient rise of interferometry radii and volume from top RHIC to LHC energies [36]. It is important to note that utilization of hydrokinetic model in between pure hydrodynamics and UrQMD gives the possibility to switch correctly to the UrQMD cascade at any space-like hypersurface, in particular, at isochronic one. It allows one to avoid problems that usually appear in hybrid models matching hydrodynamics with hadronic cascade at hadronisation hypersurface. The latter typically contains

nonspace-like sectors that cannot be correctly accounted for in initial conditions for hadronic cascade model.

In the recent paper [39] the correlation femtoscopy analysis is going beyond the model of independent particle emitters, which is fairly good for the systems formed in heavy ion collisions but not for small systems (with sizes about 1 fm) created in $p + p$, $p + Pb$, and $e^+ + e^-$ collisions. It is found that the uncertainty principle leads to (partial) indistinguishability of closely located emitters that fundamentally impedes their full independence and incoherence. The partial coherence of emitted particles is because of the quantum nature of particle emission and happens even if there is no specific mechanism to produce a coherent component of the source radiation. The found effect leads to reduction of the interferometry radii and suppression of the Bose-Einstein correlation functions. We review briefly the observed results and their application [40] to $p + p$ collisions at $\sqrt{s} = 7$ TeV LHC energy.

As for the elementary particle collisions, like $p + p$, there is no unambiguous interpretation of the HBT radii p_T -dependence. It became clear [41–43] that for relatively small systems the additional two-particle correlations affect the correlation functions in the kinematic region where quantum statistical (QS) and final state interaction (FSI) correlations are usually observed. These correlations can be induced by total energy and momentum conservation laws (see, e.g., [44, 45]) and minijets [39, 46, 47]. As opposed to the QS and FSI correlations, which are familiar from the correlation femtoscopy method and so are sometimes called femtoscopy correlations, these correlations are not directly related to the spatiotemporal scales of the emitter and are therefore called nonfemtoscopic correlations. Since the latter noticeably affects correlation functions for small systems, the interferometry radii extracted from the complete correlation function in $p + p$ collisions depend strongly on the assumption about the so-called correlation baseline—the strength and momentum dependence of the nonfemtoscopic correlations [41–43]. It has an influence on the interpretation of the momentum dependence of the interferometry radii in $p + p$ collisions, where the possibility of hydrodynamic behavior of matter is questionable.

2. Escape Function Dynamics of Expanding Medium Particlization

Let us start with discussion of hydrokinetic approach to $A + A$ collisions and explain how it helps switch from hydrodynamical expansion to molecular dynamics of hadronic particles. It was proposed in [35] to describe the hadronic momentum spectra in $A + A$ collisions basing on the escape function of particles which are gradually liberated from hydrodynamically expanding systems. The escape function, first introduced in hydrodynamic framework in [48, 49] without a resort to the Boltzmann kinetics, was utilized in [35] within the Boltzmann equations in a specific approximation based on hydrodynamic approach. It was shown that such a picture corresponds to a relativistic kinetic equation with the relaxation time approximation for the collision term, where the relaxation time tends to infinity, $\tau_{\text{rel}} \rightarrow \infty$, when

$t \rightarrow \infty$, indicating a gradual transition to the free-streaming regime. It is worth noting that the hydrodynamics at fairly large times play no role in formation of locally anisotropic particle spectra.

The Boltzmann equation for the distribution function $f(x, p)$ in the case of no external forces has the form

$$\frac{p^i}{p^0} \frac{\partial f(x, p)}{\partial x^i} = F^{\text{gain}}(x, p) - F^{\text{loss}}(x, p). \quad (1)$$

The terms F^{gain} and F^{loss} are associated with number of particles which, correspondingly, came to point (x, p) and left this point because of collisions. Term $F^{\text{loss}}(x, p) = R(x, p)f(x, p)$ can easily be expressed in terms of the rate of collisions of the particle with momentum p , $R(x, p) = \langle \sigma v_{\text{rel}} \rangle n(x)$. The term F^{gain} has, in general, more complicated integral structure and depends on differential cross-section.

The escape fraction, $f_{\text{esc}}^\sigma(x, p)$, describes the (probabilistic) distribution of the particles that reaches the hypersurface σ without interactions. At asymptotic hypersurface σ where times $t \rightarrow \infty$, the distribution function corresponds to free quanta: $f_{\text{esc}}^\sigma(x, p) \rightarrow f(x, p)$. In general cases, which we will need, when the space-like hypersurface σ is situated at the final times, we define the escape function as

$$f_{\text{esc}}^\sigma(x, p) = \mathcal{P}_\sigma(x, p) f(x, p), \quad (2)$$

where $\mathcal{P}_\sigma(x, p)$ is the escape probability for particle to reach freely the hypersurface σ at some point $(t_\sigma, \mathbf{x}_\sigma)$ starting from the point (t, \mathbf{x}) . If the point x belongs to this hypersurface σ , then $\mathcal{P}_\sigma(x, p) = 1$, and so

$$f_{\text{esc}}^\sigma(x, p)|_\sigma = f(x, p)|_\sigma. \quad (3)$$

The escape probability is the relativistic invariant and can be expressed explicitly through the rate of collisions along the world line of free particle with momentum p :

$$\mathcal{P}_\sigma(x, p) = \exp\left(-\int_t^{t_\sigma} d\bar{t} R(\bar{x}, p)\right), \quad (4)$$

where $\bar{x} \equiv (\bar{t}, \mathbf{x}_\sigma + (\mathbf{p}/p_0)(\bar{t} - t_\sigma))$. It satisfies the differential equation

$$\frac{1}{\mathcal{P}_\sigma(x, p)} \frac{p^\mu}{p^0} \frac{\partial}{\partial x^\mu} \mathcal{P}_\sigma(x, p) = R(x, p) = \frac{F^{\text{loss}}(x, p)}{f(x, p)}. \quad (5)$$

It follows from (1) and (5) that

$$\frac{p^\mu}{\mathcal{P}_\sigma} \frac{\partial}{\partial x^\mu} f_{\text{esc}}^\sigma(x, p) = \mathcal{P}_\sigma(x, p) F^{\text{gain}}(x, p). \quad (6)$$

The formal solution of (6) can be presented in the following form:

$$f_{\text{esc}}^\sigma(x, p) = f_{\text{esc}}^\sigma(x_0, p) + \int_{t_{\sigma_0}(\mathbf{x}_0)}^t dt' \mathcal{P}_\sigma(x', p) F^{\text{gain}}(x', p), \quad (7)$$

where $x = (t, \mathbf{x})$, $\sigma : t = \text{const}$, $f_{\text{esc}}^\sigma(x_0, p)$ with $x_0 \equiv (t_{\sigma_0}(\mathbf{x}_0), \mathbf{x}_0 = \mathbf{x} + (\mathbf{p}/p_0)(t_{\sigma_0}(\mathbf{x}_0) - t))$ corresponds to the portion of the system, which propagates without collisions until some time t starting from initial hypersurface σ_0 , $x' \equiv (t', \mathbf{x} + (\mathbf{p}/p_0)(t' - t))$.

The expression (7) for escape function $f_{\text{esc}}^\sigma(x, p)$ can be explained in simple heuristic way as follows. Let us split the distribution function at each space-time point into two parts: $f(x, p) = f_{\text{int}}^\sigma(x, p) + f_{\text{esc}}^\sigma(x, p)$, $x = (t, \mathbf{x})$. The first part, $f_{\text{int}}^\sigma(x, p)$, describes the fraction of the system which will continue to interact before reaching the hypersurface σ . The second fraction, $f_{\text{esc}}^\sigma(x, p)$, describes the particles that reach the hypersurface σ without interactions. Denote again by $x' \equiv (t', \mathbf{x} + (\mathbf{p}/p_0)(t' - t))$ the space-time point where the particle at x with momentum p would be, if it moved freely. Consider, at each vicinity of the phase-space point (x, p) , the number of particles that have escaped from the interacting system during the time interval $(t', t' + dt')$. First, this *additional* portion of escaped particles can be produced only from the interacting part of the system. Second, these particles are only among particles that came to the phase-space vicinity of the point (x', p) *just after* the interaction during the time dt' . Indeed, if some particles from the interacting part of the system $f_{\text{int}}^\sigma(x', p)$ do not interact during the given time interval $(t', t' + dt')$, then they will interact without fail at some future time; thus, they cannot contribute to the additional portion of particles escaping during dt' . Therefore, the additional contribution $\Delta f_{\text{esc}}^\sigma(x, p; t')$, from the time interval $(t', t' + dt')$ to the distribution function $f_{\text{esc}}^\sigma(x, p)$, is $\Delta f_{\text{esc}}^\sigma(x, p; t') = \mathcal{P}_\sigma(x', p) F^{\text{gain}}(x', p) dt'$ for $t' < t$ and is zero for $t' > t$. Here $\mathcal{P}_\sigma(x', p)$ is probability for any *given* particle at point x' with momentum p to reach without interaction the hypersurface σ . The summation of such contributions is presented by (7), and the differential of this equation leads to (6).

Utilization of the escape function for the momentum spectra formation is based on (3) which can be used to describe inclusive spectra of particles,

$$p^0 \frac{dN}{dp} = \langle a_p^+ a_p \rangle, \quad p_1^0 p_2^0 \frac{dN}{d\mathbf{p}_1 d\mathbf{p}_2} = \langle a_{p_1}^+ a_{p_2}^+ a_{p_1} a_{p_2} \rangle, \dots, \quad (8)$$

that are constructed in the standard way by means of the averages of product of creation and annihilation operators. Namely, on the hypersurface σ_{out}

$$\langle a_{p_1}^+ a_{p_2} \rangle = \int_{\sigma_{\text{out}}} d\sigma_\mu(x) p^\mu \exp(iqx) f_{\text{esc}}(x, p), \quad (9)$$

where $p = (p_1 + p_2)/2$, $q = p_1 - p_2$. Then, using the Gauss theorem, (6) and (1) analytically continued to

off-mass-shell four-momenta p , and taking into account that $\partial_\mu(p^\mu \exp(iqx)) = 0$ for particles on mass shell, one can get

$$\begin{aligned} \langle a_{p_1}^+ a_{p_2} \rangle &= p_0 \int_{\sigma_0} d^3 \sigma_\mu(x_0) p^\mu f_{\text{esc}}^\sigma(x_0, p) e^{-iqx_0} \\ &+ p_0 \int_{\sigma_0} d^4 x \mathcal{P}_\sigma(x, p) F^{\text{gain}}(x, p) e^{-iqx}, \end{aligned} \quad (10)$$

$$\begin{aligned} \langle a_{p_1}^+ a_{p_2} \rangle &= p^0 \int_{\sigma_0} d^3 \sigma_\mu(x_0) p^\mu f(x_0, p) e^{-iqx_0} \\ &+ p^0 \int_{\sigma_0} d^4 x \\ &\times [F^{\text{gain}}(x, p) - F^{\text{loss}}(x, p)] e^{-iqx}, \end{aligned} \quad (11)$$

respectively, where $\mathcal{P}_{\sigma_{\text{out}}}(x, p)$ is the probability for particle to reach the hypersurface σ from the space-time point x , $f_{\text{esc}}^\sigma(x_0, p) = f(x_0, p) \mathcal{P}_\sigma(x_0, p)$ is a portion of the particles at the initial hypersurface σ_0 that reach hypersurface σ moving freely without interactions, $f(x_0, p)$ is the distribution function at σ_0 , and $p^0 \mathcal{P} F^{\text{gain}}$ is the Lorentz-invariant emission density.

The hydrokinetic approach is based on (10) where one utilizes the escaping function dynamics (6) for finding solution of the Boltzmann equation at hypersurface σ and calculation there the particle momentum spectra. The escaped functions and escape probabilities are calculated within the local equilibrium approximation for the term F^{gain} and the collision term R . The latter is defined from the particle cross-sections which are similar to those in the UrQMD. The equation of state is supposed to be the same as in the Boltzmann hadron gas with changing in time chemical composition. The evolution of the parameters, such as the temperature, chemical potentials, particle concentrations, and collective velocities in the hadron-resonance gas, are defined by the equations of relativistic hydrodynamics. All the details are presented in [23, 29, 35]. The resulting distribution function at σ , found from the integral form (7) of the equation for escaped functions, is, of course, far from the local equilibrium one.

In the models like UrQMD, distribution function dynamics (1) is utilized for calculation of the momentum spectra in accordance with (11). Both approaches coincide in the case of free-streaming, when $F^{\text{gain}}(x, p) = F^{\text{loss}}(x, p) \equiv 0$ and therefore $\mathcal{P}_\sigma(x_0, p) \equiv 1$, then the second terms in (10), (11) are equal to zero and the first terms are coincided (note that it is not the case when $F^{\text{gain}}(x, p) = F^{\text{loss}}(x, p) \neq 0$). Then distribution function dynamics (1) is still as at a free-streaming, while the escaping function dynamics (6) becomes nontrivial). It is worth noting that if the initial hypersurface σ_0 has non-space-like sites, $\Delta\sigma_\mu(x_1)$, then for some momenta p_1 we have $p_1^\mu \Delta\sigma_\mu(x_1) < 0$, and so these parts give the negative contribution to the particle number density according to (10) and (11). It happens because the particles are going inside the hypersurface σ_0 near the point x_1 . This negative contribution will

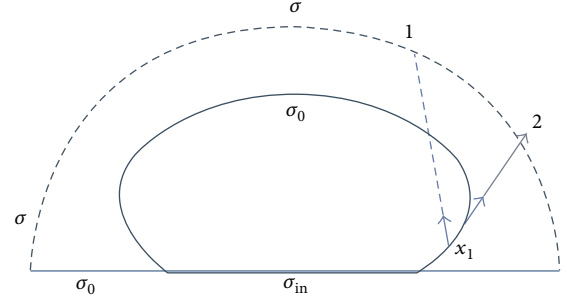


FIGURE 1: The cartoon of the particleization at the hypersurface σ_0 (solid line) and spectra formation at σ (dashed line). The very initial system forms at the hypersurface σ_{in} (double line) and then evolves. The Gauss theorem in (10) and (11) is applied to enclosed hypersurface $\sigma_0 \oplus \sigma$. In the case of large opacity $f_{\text{esc}}^\sigma(x_1, p_1) \approx 0$ for particle 1, also is small for particle 2, and so $p_\mu \Delta\sigma_0^\mu(x_1) f_{\text{esc}}^\sigma(x_1, p) \approx 0$, while for the distribution function $f(x_1, p)$ the similar value $p_\mu \Delta\sigma_0^\mu(x_1) f(x_1, p)$ is not zero, and for $p = p_1$ it is negative if $\Delta\sigma_0$ is a non-space-like site of the hypersurface σ_0 .

be compensated when the particle crosses the hypersurface again in another point x_2 of the hypersurface to go out. See the possible trajectory of the particle 1 in Figure 1. Of course, the Gauss theorem applied to the enclosed hypersurface $\sigma_0 \oplus \sigma$ guarantees the correct positive result for particle momentum spectra, no matter how complicated structure σ_0 has and how many times the negative contributions happen. As for the external hypersurface σ , it can be chosen as a space-like one.

Typically at a modeling of $A + A$ collisions the initial conditions for the Boltzmann equations are selected at the hypersurface σ_0 close to the hadronisation hypersurface. Such a hypersurface is not everywhere a space-like one, but at sites with $p^\mu \Delta\sigma_\mu < 0$ particles cannot go deeply inside because of high opacity (see Figure 1). It is taken into account in the escape function formalism, where the escape probability for the particles with momentum directed into the fluid is about zero at these sites, $\mathcal{P}_\sigma(x_0, p) \approx 0$, and so the escape function is about zero, $f_{\text{esc}}^\sigma(x_0, p) \approx 0$, resulting in suppression of the negative contributions to particle momentum density in (10) from the σ_0 hypersurface. Note that within the escape function formalism a transition from continuous medium to particles is described as a gradual process, because escape function and escape probability can be defined for both sides of the hypersurface σ_0 (in other words, hadronisation process is treated as gradual in the escape function dynamics, and the very initial system state is defined, in fact, on a space-like hypersurface). The latter fact, accounting for (2), implies the continuity of the distribution function through σ_0 in accordance with Boltzmann kinetics (1). It means that if it is the local equilibrium on the one side of the hypersurface, it will be the same on the other side, no matter whether they are space-like or non-space-like sectors. Then in (11), dealing with the full distribution function, the negative contributions at the non-space-like sites really exist and have to be preserved to maintain true dynamics. Summarizing, the hydrokinetic model is based on continuous behavior of the physical values. It implies a continuous

behavior of the locally isotropic distribution function at any parts of the hypersurface σ_0 , including “bad” nonspace-like sites. It is implemented through a continuous hydrodynamic description of the matter crossing the σ_0 that is utilized for calculation of the escape probability and emission function. Therefore no discontinuity in the energy and momentum flows through σ_0 arises. The hydrokinetic approach accounts also for the smooth time behavior of the escape function that forms the distribution function at some space-like hypersurface σ that can be used then to provide the input of the nonlocally equilibrium distribution function (the output of HKM) to the UrQMD [30].

In cascade models, which solve the Boltzmann equation in the form (II), one does not deal with the small fraction of the particles that are already free at σ_0 but brings into play the distribution function $f(x, p)$ itself for further numerical simulations of the collisions in the Boltzmann gas. Then one can see from (II) that near the nonspace-like site at x_1 a negative number of the particles with corresponding momenta p_1 has to be “injected” (see Figure 1). Typically, to cure this dilemma people just cut them in the full distribution function $f(x_1, p)$, that leads to discontinuity of the energy and momentum flows through the corresponding sites of σ_0 [50]. Such a cut, introduced through the Heaviside function $\Theta(d\sigma_\mu p^\mu)$ in the Cooper-Frye prescription [51], destroys the basic equation (II) where the negative contributions have to be preserved! Also locally, it obviously violates the continuity of the particle current $n^\mu = nu^\mu : \partial_\mu n^\mu(x)|_{\Delta\sigma_0(x_1)} \neq 0$. The error of such prescription is that it considers a decaying hadronic system rather as a star, practically unlimited reservoir of emitted photons/particles, while the hadronic medium formed in the heavy ion collisions is a small compact holder of emitted particles and it is rearranged when the system loses them (back reaction).

The situation can be improved if one introduces some model of the surface layer with the locally isotropic thermal distribution that includes also the particles with momenta p_1 moving towards the nonspace-like sites where $p_1^\mu \Delta\sigma_0(x_1) < 0$. These particles have to collide with the particles that move from the inside of $\Delta\sigma_0(x_1)$ to outside. The attempt to substitute such real collisions inside the surface layer by the elastic reflection from the moving (with the “velocity” of the nonspace-like site) wall was performed in [52]. It results in the specific combination of the Heaviside Θ -functions in the Cooper-Frye formula and provides the local conservation law for particles $\partial_\mu n^\mu(x)|_{\Delta\sigma_0(x_1)} = 0$. Such a prescription is utilized in the FAST MC Freeze-out Generator [53] and is planned to be used in UrQMD [54]. However, the method [52] ensures continuity of particle and energy flows but not the momentum flow and so preserves discontinuity of momentum-energy tensor at nonspace-like segments of σ_0 [52].

Because of the difficulties in building the model of the surface layer, one can use hydrokinetics, that does not deal directly with the distribution function at σ_0 but only with the distributions of particles continuously escaping from the hydrodynamically expanding matter and calculate a nonequibrated distribution function with (2) and (4) on

a space-like hypersurface σ where one can switch to UrQMD cascade without troubles described.

Theoretical calculations, presented in the next section, are performed in hybrid hydrokinetic model (hHKM) [30]. At the initial state the Monte-Carlo Glauber model of the initial conditions is used (see [30]). After the thermalization stage of the system’s evolution, the matter is supposed to be chemically and thermally equilibrated, and its expansion is described within perfect $(2+1)D$ boost-invariant relativistic hydrodynamics with the lattice QCD-inspired equation of state in the quark-gluon phase [55] matched with chemically equilibrated hadron-resonance gas via crossover-type transition. The hadron-resonance gas consists of 329 well-established hadron states (according to Particle Data Group compilation [56]) made of u , d , and s quarks, including σ -meson ($f_0(600)$). With such an equilibrated evolution the system reaches the chemical freeze-out isotherm with the temperature $T_{\text{ch}} = 165$ MeV. At the second stage with $T < T_{\text{ch}}$, the hydrodynamically expanding hadron system gradually loses its (local) thermal and chemical equilibrium, and particles continuously escape from the system. This stage is described within the hydrokinetic approach [35] to the problem of dynamical decoupling. In hHKM model [30] the hydrokinetic stage is matching with hadron cascade UrQMD one [37, 38] at the isochronic hypersurface $\sigma : t = \text{const}$ (with $T_\sigma(r = 0) = T_{\text{ch}}$) that guarantees the correctness of the matching (see [29, 30] for details). In the latter case of transition from the hydrokinetics to cascade, the following distribution functions are used:

$$\begin{aligned}
 f_i(\tau, \vec{x}, \vec{p}) &= f_i^{\text{leq}}(\tau_0, \vec{x}^{(\tau_0)}(\tau), \vec{p}) \\
 &\times \exp\left(-\int_{\tau_0}^{\tau} \tilde{R}_i(s, \vec{x}^{(s)}(\tau), \vec{p}) ds\right) \\
 &+ \int_{\tau_0}^{\tau} d\lambda \left[f_i^{\text{leq}}(\lambda, \vec{x}^{(\lambda)}(\tau), \vec{p}) \right. \\
 &\quad \times \tilde{R}_i(\lambda, \vec{x}^{(\lambda)}(\tau), \vec{p}) \\
 &\quad \left. + \tilde{G}_i^{\text{decay}}(\lambda, \vec{x}^{(\lambda)}(\tau), \vec{p}) \right] \\
 &\times \exp\left(-\int_{\lambda}^{\tau} \left[\tilde{R}_i(s, \vec{x}^{(s)}(\tau), \vec{p}) \right. \right. \\
 &\quad \left. \left. + \tilde{D}_i(s, \vec{x}^{(s)}(\tau), \vec{p}) \right] ds\right).
 \end{aligned} \tag{12}$$

The different terms in (12) correspond to the following: $\tilde{R}_i(\lambda, \vec{x}, \vec{p})$ is the collision rate of the i th sort of hadrons with the rest of particles, $\tilde{G}_i^{\text{decay}}(\lambda, \vec{x}, \vec{p})$ is an income of particles into the phase-space point owing to resonance decays, and $\tilde{D}_i(\lambda, \vec{x}, \vec{p})$ is the decay rate of a given resonance species. To calculate the collision rates, we assume meson-meson, meson-baryon, and baryon-baryon cross-sections in a way similar to the UrQMD code [37, 38].

3. Femtoscopic Correlations in Relativistic $A + A$ Collisions

In the processes of multiparticle production the two-particle correlation function is defined through the ratio of the one- and two-particle (semi)inclusive spectra as follows:

$$C(p_1, p_2) = \frac{p_1^0 p_2^0 (dN/d\mathbf{p}_1 d\mathbf{p}_2)}{p_1^0 (dN/d\mathbf{p}_1) p_2^0 (dN/d\mathbf{p}_2)}. \quad (13)$$

Experimentally, the two-particle correlation function is defined as the ratio of the distribution of particle pairs from the same collision event to the distribution of pairs with particles taken from different events. In heavy ion collisions almost all the correlations between identical pions with low relative momentum are due to quantum statistics and final state interactions. As for the latter, in this review we suppose that they are already extracted from the total correlation function (the method is well known and has been proposed in [57]).

The quantum-statistical enhancement of the pairs of identical pions produced with close momenta was observed first in $\bar{p} + p$ collisions in 1959 [58]. It took more than a decade to develop the method of pion interferometry microscope based on the discovered phenomenon. This was done at the beginning of 70s by Kopylov and Podgoretsky [4–6]. Their theoretical analysis assumed the radiating source to consist of independent incoherent emitters. In fact, such a representation is used for a long time for the analysis of the space-time structure of particle sources. For such chaotic sources the four-point average in (8) can be decomposed in the following sum of pair products:

$$\langle a_{p_1}^+ a_{p_2}^+ a_{p_1} a_{p_2} \rangle = \langle a_{p_1}^+ a_{p_1} \rangle \langle a_{p_2}^+ a_{p_2} \rangle + \langle a_{p_1}^+ a_{p_2} \rangle \langle a_{p_2}^+ a_{p_1} \rangle. \quad (14)$$

Then using (8) and (10) one can express the correlation function (13) for chaotic sources

$$C(p, q) = 1 + \frac{\int d^4 x_1 d^4 x_2 S(x_1, p) S(x_2, p) e^{iq(x_1 - x_2)}}{\left(\int d^4 x_1 S(x_1, p_1)\right) \left(\int d^4 x_2 S(x_2, p_2)\right)}, \quad (15)$$

where $p = (p_1 + p_2)/2$, $q = p_1 - p_2$, $S(x, p)$ is the emission function; if $f_{\text{esc}|\sigma_0}^\sigma \approx 0$, then $S(x, p) = p^0 F^{\text{gain}}(x, p) \mathcal{P}_\sigma(x, p)$ as it follows from (10) (in general case it includes in addition the contribution from σ_0).

When calculating these femtoscopic correlation functions in a quasiclassical particle production model (or event generator) that produces particles without any quantum correlations, the output of event generator is the list of particle positions (at the point of their last interaction) and their momenta, and $C(p, q)$ is equal to unity there. So one has to construct in addition a numerical procedure to calculate quantum-statistical correlations in accordance with (15). It is done usually in a way that is similar to the final state interaction method: one takes outcome of a given classical event generator and then constructs a numerical approximation of (15) based on smoothness conditions [59]. This can be done using the binning technique, also used in several event

generators [53, 60] including hHKM. One takes outcome of a given distribution of the particle pairs in the bins according to their relative momentum \vec{q} and the average momentum of the particle pair \vec{p} . If one calculates the correlations arising only due to the Bose-Einstein enhancement, for example, for pion pairs, the corresponding numerical equivalent of (15) at each transverse p_T bin looks like

$$C(\vec{q}) = \frac{\sum_i \sum_{j \neq i} \delta_\Delta(\vec{q} - \vec{p}_i + \vec{p}_j) (1 + \cos((p_j - p_i)(x_j - x_i)))}{\sum_i \sum_j \delta_\Delta(\vec{q} - \vec{p}_i + \vec{p}_j)}, \quad (16)$$

where $\delta_\Delta(x) = 1$ if $|x| < \Delta p/2$ and 0 otherwise, with Δp being the bin size in histograms. We decompose the relative momentum \vec{q} into $(q_{\text{out}}, q_{\text{side}}, q_{\text{long}})$ projections and perform analysis in the longitudinal center of mass system (LCMS), where the mean longitudinal momentum of the pair vanishes. Evaluation according to (16) can be done with the help of 3D histograms, implemented in ROOT library classes [61], and in hHKM two separate histograms are used to calculate the numerator and the denominator of (16), which are divided one by another to get the correlation function.

Some remarks to such a receipt are in order here. First, note that this procedure does not change single-particle momentum spectra, while one can expect that they will be changed if the quantum statistics were taken into account in the event generators. Even if hydrodynamic evolution accounts for the quantum statistics through corresponding EoS and gives Bose-Einstein and Fermi-Dirac heat distributions as the input for event generator like UrQMD, the subsequent quasiclassical UrQMD hadronic cascade destroys the true quantum-statistical picture. Unfortunately, an account for the quantum statistics is still not realized for realistic event generators because, in particular, any direct account of quantum statistics is very time consuming (for current developments and recent attempts to overcome this problem see [62, 63] and references therein). Therefore, the theoretical analysis of the quantum effects at multiparticle production, that goes beyond the simple prescription (16), is still very important. Some significant results have been already obtained. One of them concerns quantum corrections to spectra and correlations in the case when homogeneity length λ in the system is less than the particle wavelength, $\lambda < 1/p^0$ [15, 16, 64, 65]—this drastically changes the form of the spectra and BE correlations. The other is the multibosonic effects when particle number is close to the Bose-Einstein condensation [65–67]—this leads to decrease of the interferometry radii. Also, the effects of coherence for femtoscopic correlations of charged particles were considered in detail in [68] based on the formalism of generalized coherent states—it gives the tool for the correlation search of a coherence component by measuring the correlations between like and oppositely charged pions. One more quantum effect, which also cannot be taken into account by prescription (16), is connected with the uncertainty principle and is analyzed very recently in [39, 40]. We will discuss this effect in Sections 4 and 5.

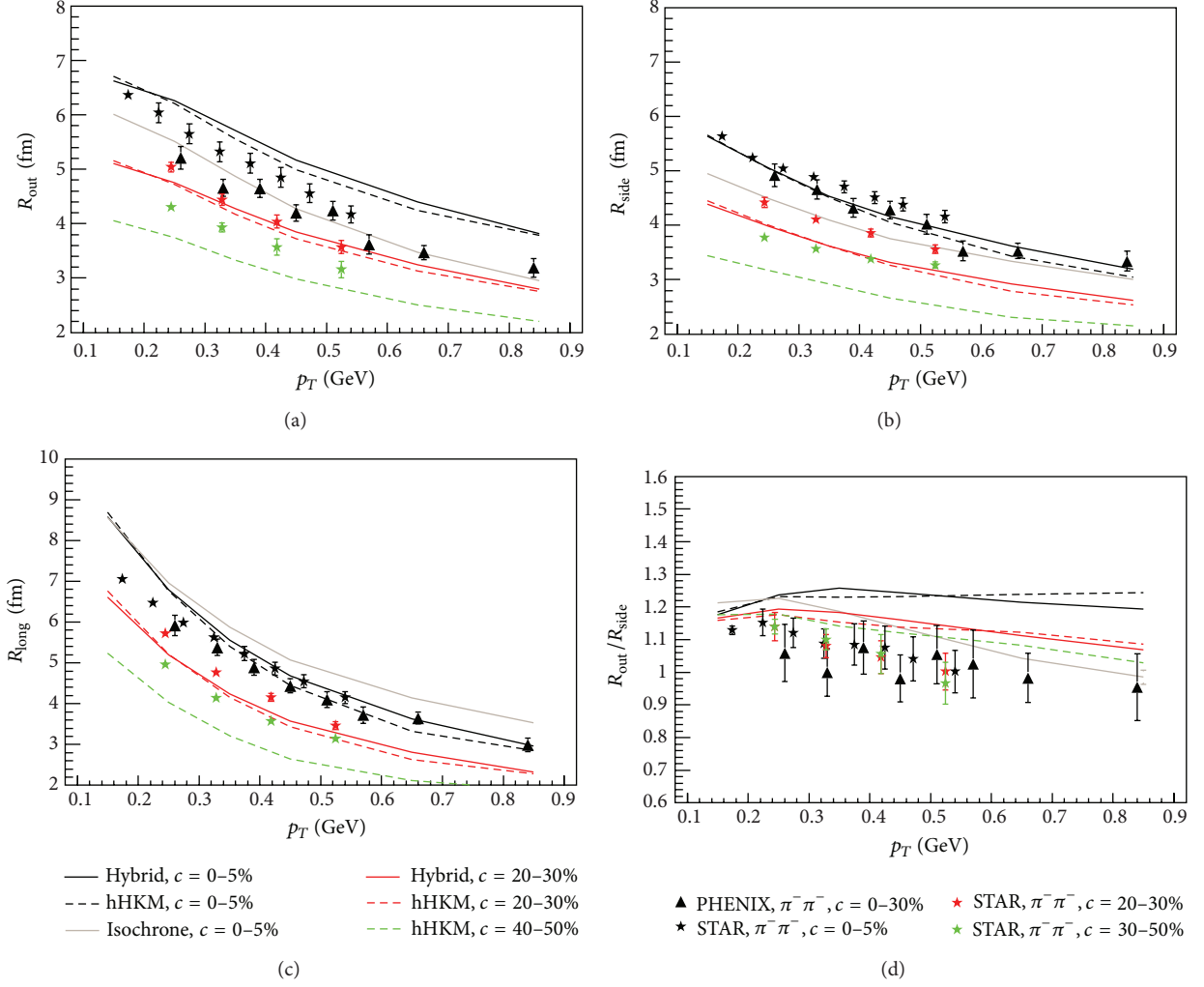


FIGURE 2: HBT radii of π^- pairs at 200 A GeV RHIC energy, calculated in different models and compared to experimental data from the STAR [69] and PHENIX [70] collaborations. Dashed lines correspond to the hydrokinetic procedure of matching (hHKM), while solid lines stand for the “hybrid” model case. The results for the “hybrid-isochronic” model are presented for central $c = 0-5\%$ events with a gray solid line. The ICs used for hydrodynamic evolution: $\tau_0 = 0.1$ fm/c with zero initial transverse flow and the MC-Glauber profiles for initial entropy density.

The resulting correlation function obtained with (16) is fitted with the Bertsch-Pratt parameterization

$$C(q) = 1 + \lambda \cdot \exp \left(-R_{\text{out}}^2 q_{\text{out}}^2 - R_{\text{side}}^2 q_{\text{side}}^2 - R_{\text{long}}^2 q_{\text{long}}^2 - R_{\text{os}}^2 q_{\text{out}} q_{\text{side}} - R_{\text{sl}}^2 q_{\text{side}} q_{\text{long}} - R_{\text{ol}}^2 q_{\text{out}} q_{\text{long}} \right). \quad (17)$$

Next, we show some results for the correlation radii from hHKM model. Following the experimental cuts (which are somewhat different for STAR, PHENIX, and ALICE Collaborations), we consider pions in central pseudorapidity region $|\eta| < 0.5$. Owing to longitudinal boost invariance and approximate azimuthal symmetry for the most central collisions which we consider for the present HBT studies, the cross-terms R_{os}^2 , R_{sl}^2 , and R_{ol}^2 are neglected.

The comparison of interferometry radii, calculated in hHKM with the experimental data from $\sqrt{s} = 200$ GeV $Au + Au$ collisions at RHIC, is shown in Figure 2. The parameters of the model are chosen to reproduce the basic set of observables: charged hadron density at midrapidity as a function of collision centrality [30]. Note that PHENIX presented its results for the 0–30% centrality bin, which corresponds to a smaller average multiplicity than the 0–5% STAR bin; thus PHENIX radii lie slightly below the ones calculated by STAR; in our model we observe the same tendency with the initial conditions set for 0–30% centrality.

From Figure 2 one can conclude that both the hHKM and the “hybrid” cases describe the data quite satisfactory, except for HBT radii for 30–50% centrality, which are clearly underestimated (and here we note that the hHKM results for 40–50% centrality, which describe well the hadron spectra and flow [30], seem to correspond to smaller effective system

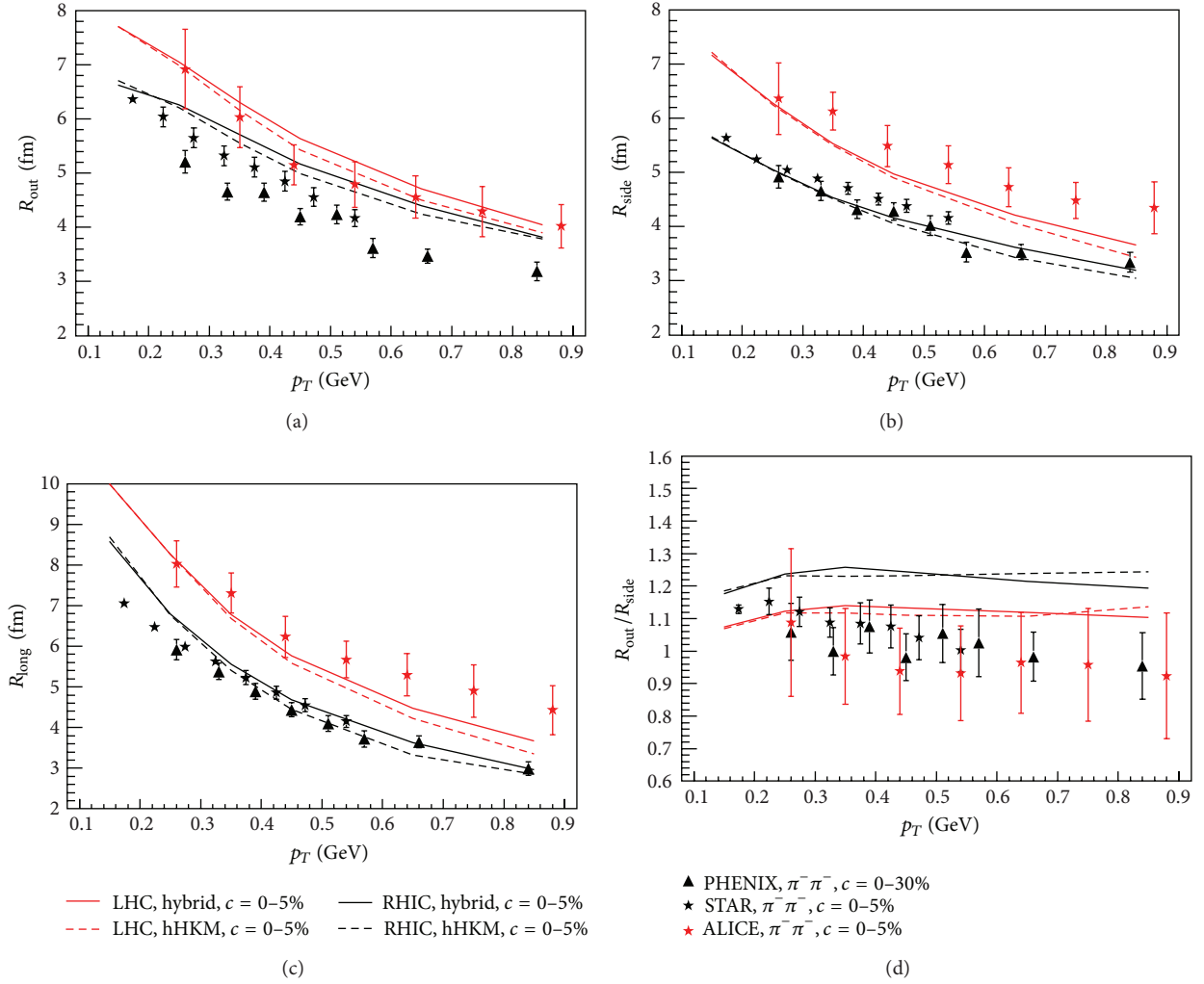


FIGURE 3: HBT radii of $\pi^- \pi^-$ pairs for the most central events, calculated in the hHKM model and compared to experimental data from ALICE [33]. Dashed lines correspond to hydrokinetic procedure of matching, while solid lines stand for the “hybrid” model case. Corresponding HBT radii for top RHIC energy are shown for comparison purposes.

size). The shear viscosity should also reduce the R_{out}/R_{side} ratio because it enhances the transverse flow, and the corresponding influence on HBT radii is shown in [71] (however the model presented in [71] does not include cascade stage; thus only resonance decays are considered after the hydrodynamic freezeout at isothermal hypersurface). As for the “hybrid-isochrone” model, it fails to describe the shape of pion, kaon, and proton transverse spectra, v_2 , and long-, side- and out-interferometry radii. The main difference between the first two (hHKM, hybrid) and “hybrid-isochrone” scenarios is that the first two matching procedures do not use the local equilibrium particle distribution functions as input for UrQMD cascade at the space-time regions where the system should be far from equilibrium. The peripheral regions at isochronic hypersurface are spatially and temporally distant from the freeze-out isotherm and have rather small temperatures, and in this transition area the finite and rapidly expanding system cannot be described hydrodynamically: the free-streaming regime of particle propagation already starts there.

Next, recent results from ALICE Collaboration show considerable rise of both R_{side} and R_{long} (and the corresponding rise of interferometric volume) with increase of collision energy from 200 A GeV RHIC to 2.76 TeV LHC. As one can see from Figure 3, this behavior is well reproduced in hHKM (see also [36]), and it is found to be caused by the protracted cascade stage at LHC energy. We keep unchanged the model parameters when passing from RHIC to LHC energies, except for a general normalization of initial entropy (or energy) density for increased dN/dy , contribution from binary collisions, and the baryonic chemical potentials at freeze-out; we also find a decent reproduction of basic set of observables with hHKM at LHC. One can conclude that this supports the same physical picture of bulk matter evolution at both top RHIC and LHC energies.

In Figure 4 (taken from recent STAR publication [72]) we show HBT radii of kaon pairs measured recently by STAR collaboration, compared to the older results by PHENIX and to the ones calculated in hHKM. The figure demonstrates

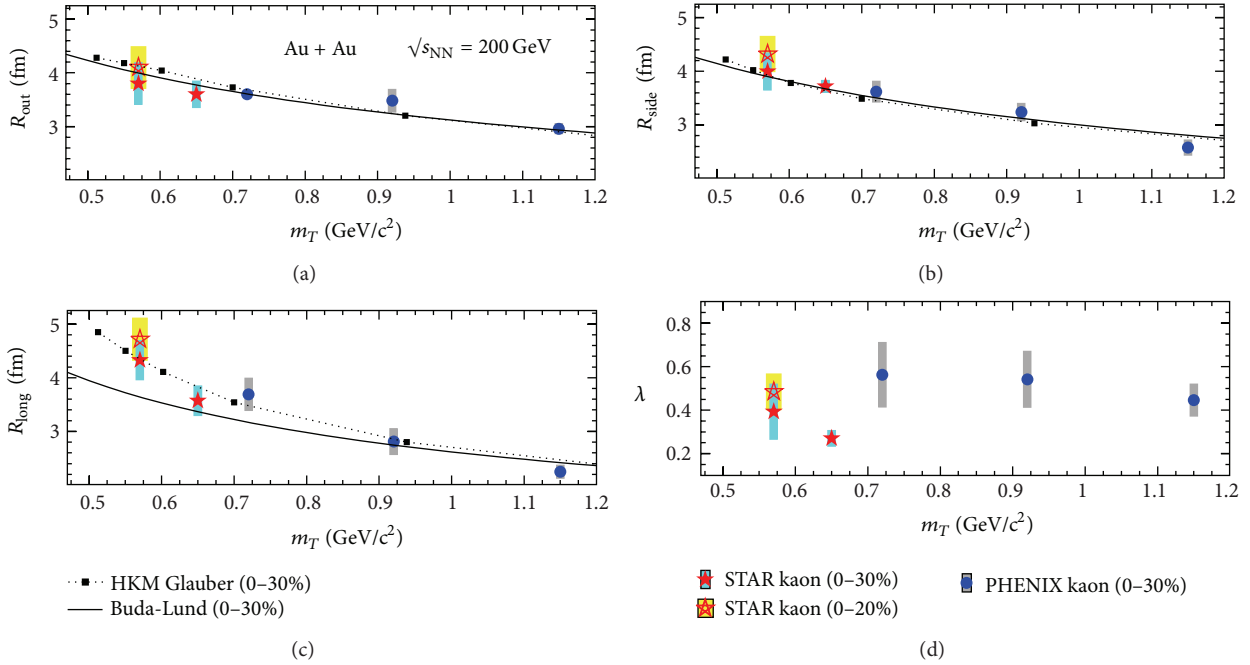


FIGURE 4: Transverse mass dependence of Gaussian radii (a) R_{out} , (b) R_{side} , and (c) R_{long} for midrapidity kaon pairs from the 30% most central Au + Au collisions at $\sqrt{s_{NN}} = 200$ GeV. The results from STAR [72] and PHENIX [73] are compared to the calculations in hHKM model (dotted lines).

a good reproduction of kaon femtoscopy in hHKM and Buda-Lund models. This is connected with the fact that in hHKM we see no exact scaling between kaon and pion radii. Generally, due to different cross-sections with the hadron mixture, pions and kaons decouple (i.e., suffer their last interactions) from the system at different times and have different contributions from strong resonance decays. It was demonstrated in the pure HKM [29] that, despite the smaller cross-section, the emission duration of kaons with the same m_T as for pions is slightly larger than for pions, at least for intermediate m_T , because the same m_T corresponds to smaller p_T for kaons (and the duration of emission process is highly p_T dependent), which results in somewhat larger values of HBT radii for kaons. Generally, HBT measurements for different particle species seem to be a valuable tool to study the details of the particle liberation process and discriminate between models of particle production.

4. Correlation Femtoscopy for Small Systems

In the work [39] it is shown that for small systems formed in particle collisions (e.g., pp , e^+e^-), where the observed interferometry radii are about 1-2 fm or smaller, the uncertainty principle does not allow one to distinguish completely between individual emission points. Also the phases of closely emitted wave packets are mutually coherent. All that is taken into account in the formalism of partially coherent phases in the amplitudes of closely spaced individual emitters. The measure of distinguishability and partial coherence is then the overlap integral of the two emitted wave packets. In thermal systems the role of corresponding coherent length

is played by the thermal de Broglie wavelength that defines also the size of a single emitter. The Monte-Carlo method (16) cannot account for such effects since it deals with classical particles and point-like emitters (points of the particle's last collision). The classical probabilities are summarized according to the event generator method (16), while in the quantum approach a superposition of partially coherent amplitudes, associated with different possible emission points, serves as the input for further calculations [39]. Such approach leads to the reduction of the interferometry radii as compared to (16). In addition, the ascription of the factor $1 + \cos((x_1 - x_2)(p_1 - p_2))$ to the weight of the pion pair in (16) is not correct for very closely located points x_1 and x_2 , because there is no Bose-Einstein enhancement if the two identical bosons are emitted from the same point [39, 74]. The effect is small for large systems with large number of independent emitters, but for small systems it can be significant, and one has to exclude the excessive contributions ("double counting" [39]) in the two-particle emission amplitude. Such corrections lead to a suppression of the Bose-Einstein correlations that is manifested as a reduction of the observed correlation function intercept as compared to one in the standard method (16).

The results of [39] are presented in the nonrelativistic approximation related to the rest frame of the source moving with four-velocity u^μ . In hydrodynamic/hydrokinetic approach the role of such a source at given pair's half-momentum bin near some value p is played by the fluid element or piece of the matter with the sizes equal to the homogeneity lengths $\lambda(p)$ [15, 16]. These lengths are extracted from the HKM simulations, namely, from the interferometry radii defined by the Gaussian fits to the correlation functions

obtained in HKM. All the pairs in procedure (1) are considered in the longitudinally comoving system (LCMS) in the boost-invariant approximation automatically selects the longitudinal rest frame of the source and longitudinal homogeneity length in this frame (it is Lorentz dilated as compared to one in the global system [13]). The femtoscopy analysis is typically related to some p_T bin, and so one needs also to determine the transverse source size in the transverse rest frame, marked by the asterisk. The corresponding Lorentz transformations do not change the *side*-homogeneity length; as for the *out*-direction, we proceed in the way proposed first in [13]. The corresponding transformations then are [13, 40]

$$\begin{aligned} R_{\text{out}}^*(p) &= R_{\text{out}}(p) \frac{\cosh y_T}{\cosh(y_T - \eta_T)}, \\ R_{\text{side}}^* &= R_{\text{side}} = \lambda_{\text{side}}, \\ R_{\text{long}}^* &= R_{\text{long}} = \lambda_{\text{long}}, \\ \lambda_{\text{out}}^* &= \lambda_{\text{out}} \frac{\cosh y_T}{\cosh(y_T - \eta_T)}, \\ \frac{P_{\text{out}}^*}{P_0^*} T^* &= T \frac{\sinh y_T}{\cosh(y_T - \eta_T)}. \end{aligned} \quad (18)$$

Here $R_{\text{out}}^{*2}(p) = \lambda_{\text{out}}^{*2} + (P_{\text{out}}^*/P_0^*)^2 T^{*2}$, T is the emission duration, η_T is a rapidity of the source in transverse direction, and $y_T = (y_{1T} + y_{2T})/2$ is half sum of transverse rapidities of the particles forming the pair. Note that $y_T^* = y_T - \eta_T$, and if rapidity of the pair is equal to the rapidity of the source, $y_T^* = 0$, then in this particular case the radius in the rest frame is Lorentz-dilated by the factor γ . Generally, the reference system where the pair's momentum is zero does not coincide with the rest frame of the source that emits the pair. Therefore the direct application of these formulas is not an easy task for rather complicated emission structure in hypothetical hydrodynamic/hydrokinetic model of $p + p$ collisions. Of course, the details of the transformation will be different for the string event generator; therefore one can estimate the theoretical uncertainties using the radii transformation just in the two limiting cases $R_{\text{out}}^* = R_{\text{out}}$ and $R_{\text{out}}^* = \gamma R_{\text{out}}$ ($\gamma = \cosh y_T$).

In [40] the quantum corrections are calculated at each p_T -bin in the rest frame of the corresponding source using (18), and then a transition is made again to the global reference system. In what follows the *asterisk* mark is omitted and all values are related to the source rest frame. To account that due to the uncertainty principle the emitters (strictly speaking emitted wave packets) have the finite sizes $\langle (\Delta x)^2 \rangle \sim k^2$ (k is the momentum variance of the particle radiation) when defining the lengths of coherence, one should at first consider the amplitude of the radiation processes and only then make statistical averaging over phases of the wave packets using the overlap integral as the coherence measure [39].

Following to [39] we present the quantum state $\psi_{x_i}(p, t)$ corresponding to a boson with mass m emitted at the time t_i

from the point \mathbf{x}_i as a wave packet with momentum variance k which then propagates freely:

$$\psi_{x_i}(p, t) = e^{ipx_i - iEt} e^{i\varphi(x_i)} \tilde{f}(\mathbf{p}), \quad (19)$$

where $\varphi(x_i)$ is some phase and \tilde{f} defines the primary momentum spectrum $f(\mathbf{p})$ that we take in the Gaussian form,

$$f(\mathbf{p}) = \tilde{f}^2(\mathbf{p}) = \frac{1}{(2\pi k^2)^{3/2}} e^{-(\mathbf{p}^2/2k^2)}, \quad (20)$$

with the variance $k^2 = mT$. The effective temperature of particle emission in the local rest frames in HKM, T , is close to the chemical freeze-out temperature T_{ch} .

The amplitude of the single-particle radiation from some 4-volume is supposed to be a superposition of the wave functions $\psi_x(p)$ with the Gaussian coefficients $\hat{\rho}(x) = \sqrt{\rho(x)}$, where $\rho(x)$ is the probability distribution in the case of random phases:

$$\rho(x, t) \propto e^{-\sum_i x_i^2/2\lambda_i^2(p) - t^{*2}/2T^{*2}(p)}. \quad (21)$$

Then in the rest frame of the source

$$A(p, t) = c \int d^4x \psi_x(p, t) \hat{\rho}(x), \quad (22)$$

where c is the normalization constant.

The single- and two-particle spectra, averaged over the ensemble of emission events with partially correlated phases $\varphi(x)$ are

$$\begin{aligned} \overline{W(p)} &= c^2 \int d^4x d^4x' e^{ip(x-x')} \hat{\rho}(x) \hat{\rho}(x') \\ &\quad \times f(\mathbf{p}) \left\langle e^{i(\varphi(x) - \varphi(x'))} \right\rangle, \\ \overline{W(p_1, p_2)} &= c^4 \int d^4x_1 d^4x_2 d^4x'_1 d^4x'_2 e^{i(p_1x_1 + p_2x_2 - p_1x'_1 - p_2x'_2)} \\ &\quad \cdot f(\mathbf{p}_1) f(\mathbf{p}_2) \hat{\rho}(x_1) \hat{\rho}(x_2) \hat{\rho}(x'_1) \hat{\rho}(x'_2) \\ &\quad \times \left\langle e^{i(\varphi(x_1) + \varphi(x_2) - \varphi(x'_1) - \varphi(x'_2))} \right\rangle. \end{aligned} \quad (23)$$

The phase averages are associated with corresponding overlap integrals [39]

$$\left\langle e^{i(\varphi(x) - \varphi(x'))} \right\rangle = G_{xx'} = I_{xx'} = \left| \int d^3\mathbf{r} \psi_x(t, \mathbf{r}) \psi_{x'}^*(t, \mathbf{r}) \right|, \quad (24)$$

$$\begin{aligned} \left\langle e^{i(\varphi(x_1) + \varphi(x_2) - \varphi(x'_1) - \varphi(x'_2))} \right\rangle &= G_{x_1x'_1} G_{x_2x'_2} + G_{x_1x'_2} G_{x_2x'_1} \\ &\quad - G_{x_1x'_2} G_{x_2x'_1} G_{x_1x_2}, \end{aligned} \quad (25)$$

where $\psi_{x_i}(t, \mathbf{r}) = (1/(2\pi)^{3/2}) \int f(\mathbf{p}) e^{-i\mathbf{p}(\mathbf{r}-\mathbf{x}_i)} e^{-i(\mathbf{p}^2/2m)(t_i-t)} d^3p$ are the wave functions of single bosonic states in coordinate representation.

Then the correlation function $C(\mathbf{p}, \mathbf{q})$ can be expressed through the homogeneity lengths in the local rest frame $R_L \equiv \lambda_{\text{long}}^*(p)$, $R_S \equiv \lambda_{\text{side}}^*(p)$, and $R_O \equiv \lambda_{\text{out}}^*(p)$ which in its turn are expressed through the HBT radii obtained from the Gaussian fit (17) of the HKM correlation functions and transformation law (18) as described above:

$$C(\mathbf{p}, \mathbf{q}) = \frac{\overline{W(p_1, p_2)}}{W(p_1)W(p_2)} = 1 + e^{-q_O^2 R_O^2 (4k_0^2 R_O^2 / (1+4k_0^2 R_O^2)) - q_S^2 R_S^2 (4k_0^2 R_S^2 / (1+4k_0^2 R_S^2))} \times e^{-q_L^2 R_L^2 (4k_0^2 R_L^2 / (1+4k_0^2 R_L^2))} \times e^{-((\mathbf{p}\mathbf{q})^2 T^2 / m^2) (4k^2 T^2 / (1+4k^2 T^2))} - C_d(\mathbf{p}, \mathbf{q}), \quad (26)$$

where $k_0^2 = k^2 / (1 + \alpha k^4 T^2 / m^2)$, parameter $\alpha(k^2 R^2)$ is defined from the model numerically (it is the order of unity for $R \sim 1$ fm and tends to zero for the large sources—see [39] for details), and the subtracted term

$$C_d(\mathbf{p}, \mathbf{q}) = e^{-2q_O^2 k_0^2 R_O^4 (1+8k_0^2 R_O^2) / (1+4k_0^2 R_O^2) (1+8k_0^2 R_O^2 + 8k_0^4 R_O^4)} \times e^{-2q_S^2 k_0^2 R_S^4 (1+8k_0^2 R_S^2) / (1+4k_0^2 R_S^2) (1+8k_0^2 R_S^2 + 8k_0^4 R_S^4)} \times e^{-2q_L^2 k_0^2 R_L^4 (1+8k_0^2 R_L^2) / (1+4k_0^2 R_L^2) (1+8k_0^2 R_L^2 + 8k_0^4 R_L^4)} \times e^{-2k^2 T^4 (\mathbf{p}\mathbf{q})^2 (1+8k^2 T^2) / m^2 (1+4p^2 T^2) (1+8k^2 T^2 + 8k^4 T^4)} \times F(k_0^2 R_i^2, k^2 T^2),$$

$$F(k_0^2 R_i^2, k^2 T^2) = \left(\frac{k_0}{k} \right)^{3/2} \times \left(\frac{(1+4k^2 T^2)}{(1+8k^2 T^2 + 8k^4 T^4)} \frac{(1+4k_0^2 R_O^2)}{(1+8k_0^2 R_O^2 + 8k_0^4 R_O^4)} \frac{(1+4k_0^2 R_S^2)}{(1+8k_0^2 R_S^2 + 8k_0^4 R_S^4)} \frac{(1+4k_0^2 R_L^2)}{(1+8k_0^2 R_L^2 + 8k_0^4 R_L^4)} \right)^{1/2} \quad (27)$$

responds for the elimination of the double counting.

Now we can see that the apparent interferometry radii extracted from the Gaussian fits to the correlation function (26) are reduced as compared to those obtained in the standard approach.

Particularly, if we neglect the double counting effects, truncate the subtracted term $C_d(\mathbf{p}, \mathbf{q})$ in (26), and fit the correlation function with the Gaussian form (17), we obtain

the femtoscopic radii R_{out} , R_{side} , and R_{long} related to the standard ones $R_{\text{out,st}}$, $R_{\text{side,st}}$, and $R_{\text{long,st}}$ as follows:

$$\frac{R_{\text{out}}^2}{R_{\text{out,st}}^2} = \left(R_O^2 \frac{4k_0^2 R_O^2}{1+4k_0^2 R_O^2} + T^2 v_{\text{out}}^2 \frac{4k^2 T^2}{1+4k^2 T^2} \right) \times (R_O^2 + T^2 v_{\text{out}}^2)^{-1}, \quad (28)$$

$$\frac{R_{\text{side}}^2}{R_{\text{side,st}}^2} = \frac{4k_0^2 R_S^2}{1+4k_0^2 R_S^2},$$

$$\frac{R_{\text{long}}^2}{R_{\text{long,st}}^2} = \frac{4k_0^2 R_L^2}{1+4k_0^2 R_L^2},$$

where $v_{\text{out}} = p_{\text{out}}^* / p_0^* \ll 1$ according to the nonrelativistic approximation. At large source sizes, for example, when the homogeneity lengths correspond to $A + A$ -collisions, $k_0^2 R^2 \gg 1$, $k^2 T^2 \gg 1$, all these ratios tend to unity.

The mean emission duration is supposed to be proportional to the average system's size, $T = a(R_O + R_S + R_L)/3$, that leads to the quadratic equation expressing R_O (and T) through $R_{i,\text{st}}$. The latter are connected with ones taken in the global reference system according to transformation laws (18). The value a is a free model parameter. Then we put these extracted values into the expression (26) for the correlation function and perform its fitting with the Gaussian (17). This gives us finally the interferometry radii R_{out} , R_{side} , and R_{long} in view of the uncertainty principle. The radii are presented then in the global system using the transformations inverse to (18).

The correlation function is the ratio of the two- and one-particle spectra. It is found [39] that quantum corrections to this ratio are not so sensitive to different forms of the wave packets as the spectra itself. In particular, the effective temperature of the *corrected* transverse spectra depends on whether the parameter of mean particle momentum is included or not into the wave packet formalism. If yes, the corrected effective temperature for small sources $R \sim 1$ fm is equal or even higher than that the individual emitters have, $T = k^2/m$, while for the wave packets in the form (19) it is lower [39]. Besides this, in the nonrelativistic approximation one can describe only very soft part of the spectra. That is why we focus in the paper on the corrections to the Bose-Einstein correlation functions where in the rest frame of the source the total and relative momenta of the boson pairs are fairly small.

5. Femtoscopy of $p + p$ Collisions in View of the Uncertainty Principle

This section of the review is based on the results of [40].

The attempt of the systematic theoretical analysis of the pion femtoscopy of $p + p$ collisions at the top RHIC and $\sqrt{s} = 0.9$ TeV LHC energies was made in [75] within Quark-Gluon String Model (QGSM). It was found that for a satisfactory description of the interferometry radii one needs to reduce significantly the formation time by increasing the string tension value relative to the one fixed by the QGSM

description of the spectra and multiplicity. Otherwise, the radii obtained within QGSM are too large as compared to the measured femtoscopy scales. Hypothetically one can hope to reduce the predicted radii suggesting the other approach—the hydrodynamic mechanism of the bulk matter production in $p + p$ collisions, at least, for high multiplicity events. Although the applicability of hydrodynamics to $p + p$ collisions is still questionable, there are certain arguments in its favor. For instance, in [76, 77] multiparticle production in nuclear collisions is related to that in hadronic ones within the model based on dissipating energy of participants and their types, which includes Landau relativistic hydrodynamics and constituent quark picture. Then to reproduce high multiplicity, the initially very small $p + p$ system has to be initially superdense. This leads to very large collective velocity gradients, and so the homogeneity lengths should be fairly small. However, as we will demonstrate, even at the maximally possible velocity gradients at the given multiplicity, one gets again an overestimate of the interferometry radii in $p + p$ collisions. Therefore, one can conclude that the problem of theoretical description of the interferometry radii in $p + p$ collisions may be a general one for different types of event generators associated with various particle production mechanisms. Here we try to correct the femtoscopic results of event generators using for this aim the quantum effects accounting for partial indistinguishability and mutual coherence described in the previous section.

We will employ the hydrokinetic model (HKM) [23, 29, 35] in its hybrid form [30] where the UrQMD hadronic cascade is considered as the semiclassical event generator at postfreeze-out (“afterburn”) stage of the hydrodynamic/hydrokinetic evolution. The analysis provided in [30] shows a fairly small difference of the one- and two-particle spectra obtained in hHKM and in the case of the direct matching of hydrodynamics and UrQMD cascade at the chemical freeze-out hypersurface. Thus, in this paper we utilize just the latter simplified “hybrid” variant for the afterburn stage.

Let us try to apply the above hydrokinetic picture to the LHC $p + p$ collisions at $\sqrt{s} = 7$ TeV aiming to get the minimal interferometry radii/volume at the given multiplicity bin. As it is known [23] the maximal average velocity gradient and so the minimal homogeneity lengths can be reached at the Gaussian-like initial energy density profile. For the same aim we use the minimal transverse scale in ultrahigh energy $p + p$ collision, close to the size of gluon spots [78, 79] in proton moving with a speed $v \approx c$. In detail, the initial boost-invariant tube for $p + p$ collisions has the energy density Gaussian distribution in transverse plane with the width (rms) $R = 0.3$ fm [78, 79], and, following [30], we attribute it to the initial proper time $\tau_0 = 0.1$ fm/c. At this time there is no initial transverse collective flow. The maximal initial energy density is defined by all charged particle multiplicity bin.

In Figures 5 and 6, taken from [40], for the two multiplicity classes $\langle dN_{\text{ch}}/d\eta \rangle = 9.2$ and $\langle dN_{\text{ch}}/d\eta \rangle = 17.9$ we present the three curves for interferometry radii as a function of p_T : the experimental one, the one taken just from the HKM simulations, and the other one obtained after application of the quantum corrections. The basic parameters

used correspond to the limiting case, when the homogeneity lengths in the source rest frame coincide with the ones taken from the model, $\gamma = 1$. For this case $a \approx 1$, $k = 0.18$ GeV/c, and $p_T^* = 0.13$ GeV/c. The α parameter values linearly increase with p_T from 1.15 to 1.35 for the $\langle dN_{\text{ch}}/d\eta \rangle = 9.2$ case and from 1.02 to 1.1 for $\langle dN_{\text{ch}}/d\eta \rangle = 17.9$. As one can see, the quantum corrected p_T -dependency of the radii gets closer to the experimental values, but for large p_T the corrections are insufficient to fully describe the observable femtoscopy scales behavior. This fact may indicate that sources of particles with large p_T cannot be described in hydrodynamical approximation. Note that just for such large p_T the nontrivial baseline corrections, already provided in presented experimental data, are very essential.

Considering the multiplicity dependence of femtoscopy scales in $p + p$ and $p + Pb$ collisions we cannot bypass the scaling hypothesis issue [44, 45], that suggests a universal linear dependence of the HBT volume on the particle multiplicity. It means that the observed interferometry volume depends roughly only on the multiplicity of particles produced in collision but not on the geometrical characteristics of the collision process. At the same time, as it was found in the theoretical analysis in [88, 89], the interferometry volume should depend not only on the multiplicity but also on the initial size of colliding systems. In more detail, the intensity of the transverse flow depends on the initial geometrical size R_0^g of the system: roughly, if the pressure is $p = c_0^2 \epsilon$, then the transverse acceleration $a = \nabla_{x_T} p / \epsilon \propto p(\mathbf{x}_T = 0) / (R_0^g \epsilon) = c_0^2 / R_0^g$. The interferometry radii R_T , that are associated with the homogeneity lengths, depend on the velocity gradient and geometrical size and for nonrelativistic transverse expansion can be approximately expressed through R_0^g , the averaged transverse velocity $\langle |v_T| \rangle$, and inverse of the temperature β at some final moment τ [17, 18, 90, 91]:

$$R_T = \frac{R^g(\tau)}{\sqrt{1 + (2/\pi) \langle |v_T| \rangle^2 \beta m_T}} \quad (29)$$

$$\approx R_0^g \left(1 + \frac{\tau^2 c_0^2}{2(R_0^g)^2} - \beta m_T \frac{\tau^2 c_0^2}{\pi^2 (R_0^g)^2} \right).$$

The result (29) for the HBT radii depends obviously on R_0^g and, despite its roughness, demonstrates the possible mechanism of compensation of the growing geometrical radii of an expanding fireball in the femtoscopy measurements. For some dynamical models of expanding fireballs the interferometry radii, measured at the final time of system’s decoupling, are coincided with the initial geometrical ones, no matter how large the multiplicity is [35, 92]. The reason for such a behavior is clear from (11): if there is no dissipation in the expanding system, $F^{\text{gain}}(t, \mathbf{x}) = F^{\text{loss}}(t, \mathbf{x})$, then the spectra and correlation functions are coincided with the initial ones. The detail study of hydrodynamically expanding systems is provided in [88, 89]. It is found that at the boost-invariant isentropic and chemically frozen evolution

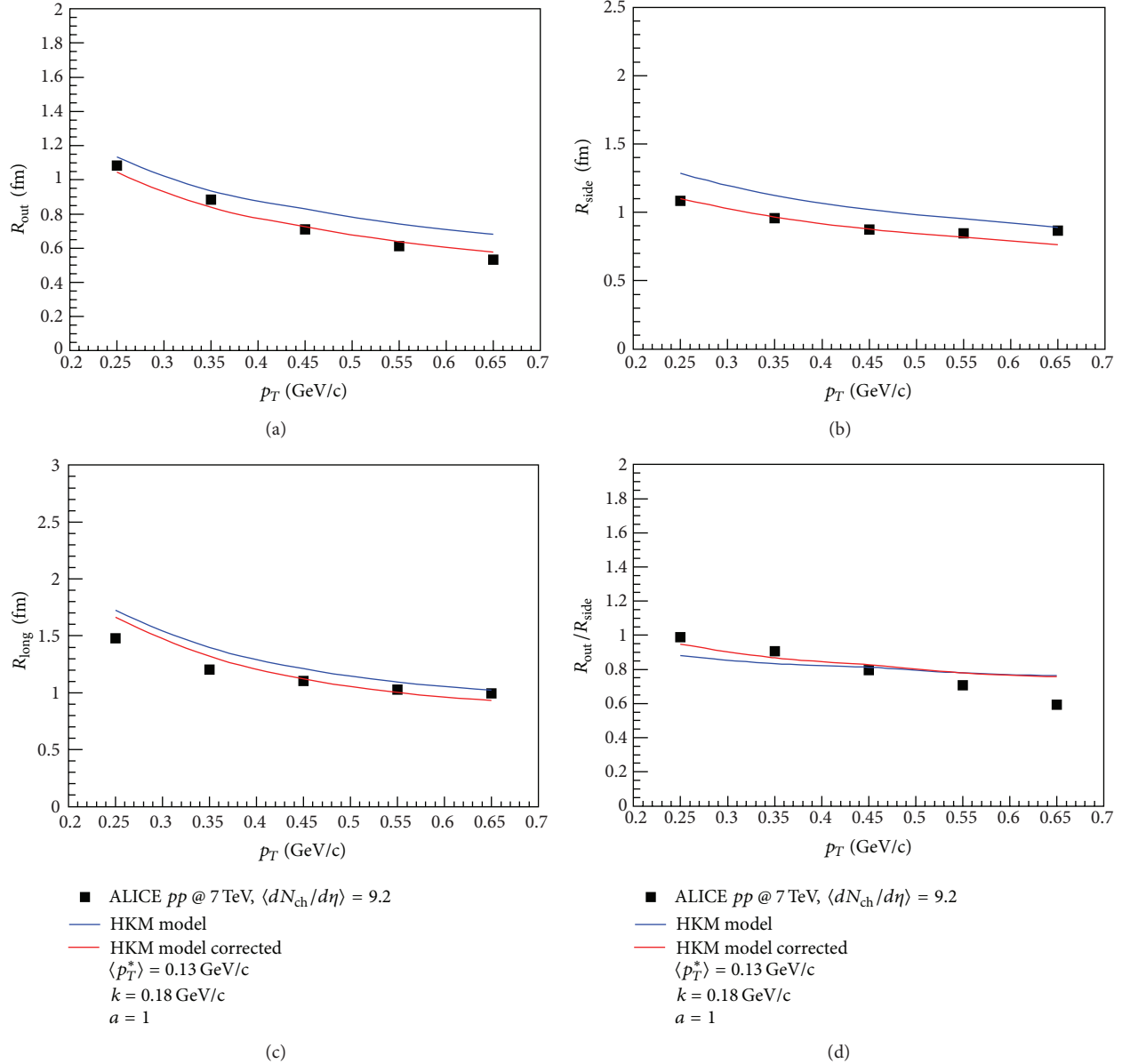


FIGURE 5: Interferometry radii dependency on p_T , $\langle dN_{ch}/d\eta \rangle = 9.2$. The data are taken from [42].

the interferometry volume, if it were possible to measure at some evolution time τ , is approximately constant:

$$V_{\text{int}}(\tau) \simeq C(\sqrt{s}) \frac{dN/dy(\tau)}{\langle f \rangle_{\tau} T_{\text{eff}}^3(\tau)}, \quad (30)$$

where $\langle f \rangle$ is the averaged phase-space density [93, 94] which is found to be approximately conserved during the hydrodynamic evolution under the above conditions as well as dN/dy [88, 89]. As for the effective temperature of the hadron spectra, $T_{\text{eff}}(\tau) = T(\tau) + m(\langle v_T(\tau) \rangle^2/2)$, one can see that, when the system's temperature T drops, the mean v_T^2 increases; therefore T_{eff} does not change much during the evolution (it slightly decreases with time for pions and increases for protons). Hence V_{int} , if it has been measured

at some evolution time τ , will also approximately conserve. Of course, the real evolution is neither isentropic nor chemically frozen and includes also QGP stage, but significant dependence of the femtoscopy scales on the initial system size preserves anyway.

Figure 7 shows the dependency $V_{\text{int}}(\langle dN_{ch}/d\eta \rangle)$ for considered case of $p + p$ collisions at the LHC, $\sqrt{s} = 7$ TeV, and for the most central (only!) collisions of nuclei having similar sizes, $Pb + Pb$ and $Au + Au$, at the SPS, RHIC, and LHC. We have also put on the plot our prediction for the interferometry volume of pPb -system, that has initially larger size than pp -system. As one can see, the different groups of points corresponding to $p+p$, $p+Pb$, and $A+A$ events cannot be fitted by the same straight line. This apparently confirms the result obtained in [88, 89] that the interferometry volume

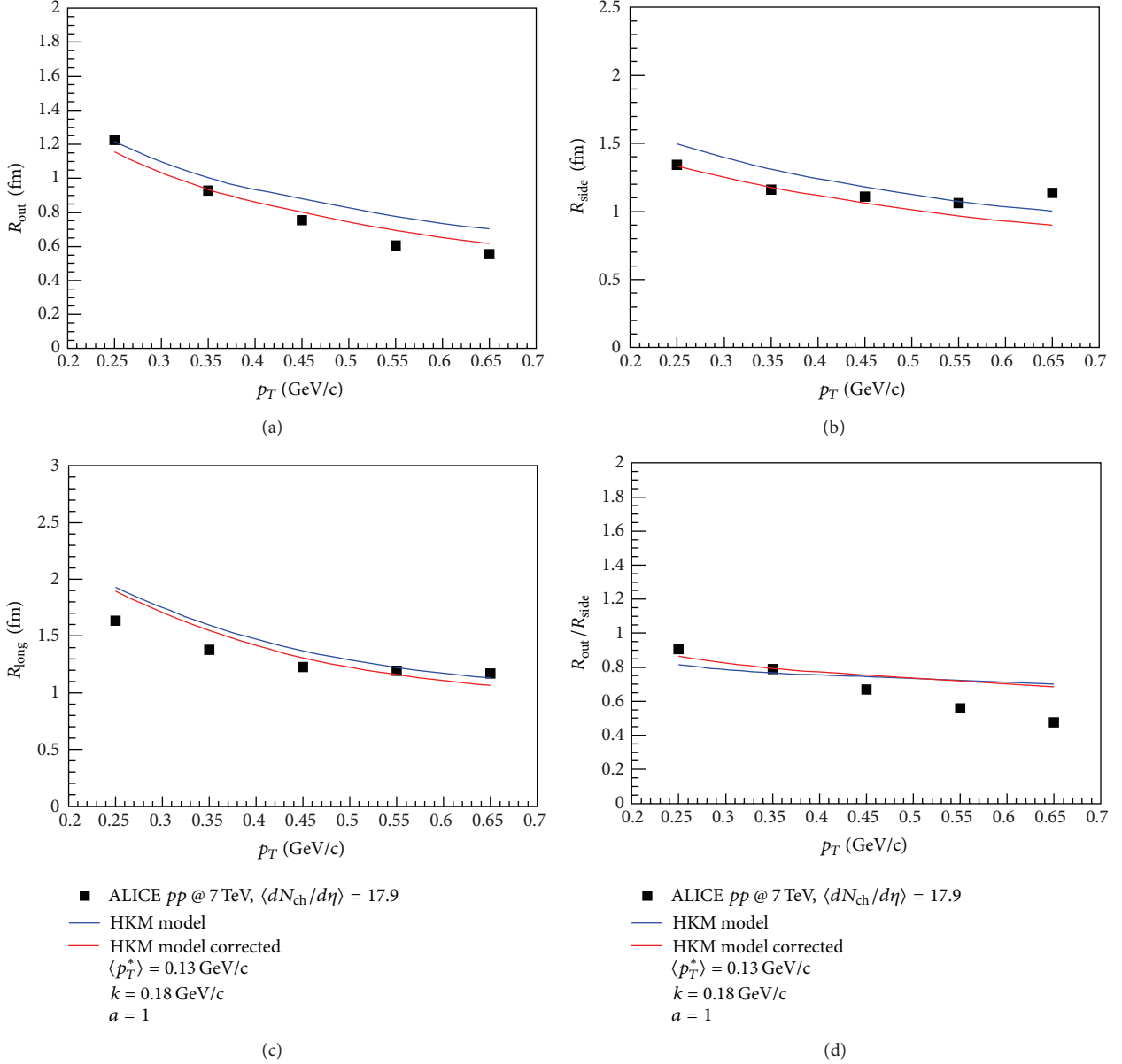


FIGURE 6: Interferometry radii dependency on p_T , $\langle dN_{ch}/d\eta \rangle = 17.9$. The data are taken from [42].

is a function of both variables: the multiplicity and the initial size of colliding system. The latter depends on the atomic number A of colliding objects and the collision centrality c .

One can conclude that quantum corrections to the pion interferometry radii in $p + p$ collisions at the LHC can significantly improve the (semiclassical) event generator results that typically give an overestimate of the experimental interferometry radii and volumes. The corrections account for the basic (partial) indistinguishability and mutual coherence of the closely located emitters because of the uncertainty principle [39]. The additional suppression of the Bose-Einstein correlation function also appears. The effects become important for small sources, 1-2 fm or smaller. Such systems cannot be completely random and so require the modification of the standard theoretical approach for

the correlation femtoscopy. The predicted femtosopic scales for $p + Pb$ collisions need some small corrections only for their minimal values corresponding to the *initial* transverse size of pPb system 0.9 fm.

6. Nonfemtoscopic Two-Pion Correlations in Small Systems

The interest to the nonfemtoscopic correlations is motivated in particular by the fact that for relatively small systems they appreciably affect the complete two-particle correlation function, forming the so-called correlation baseline. It has an influence on the interpretation of the interferometry radii momentum dependence in $p + p$ collisions with high multiplicities, where the different mechanisms of spectra

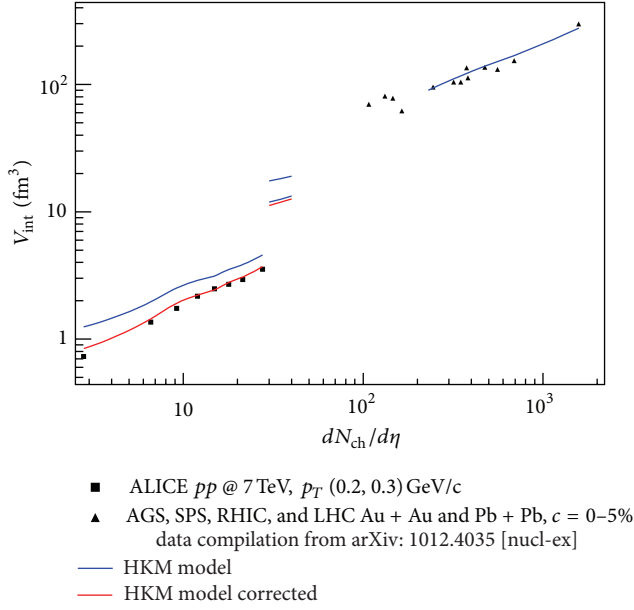


FIGURE 7: The interferometry volume dependency on charged particles multiplicity. The curve fragments in the middle correspond to the HKM prediction for $p + Pb$ collision at the LHC energy $\sqrt{s} = 5.02$ GeV. The upper one is related to the initial transverse system size $R = 1.5$ fm and for the two lower ones $R = 0.9$ fm. The curves at the left and at the right represent the HKM results for $p + p$ and $A + A$ central collisions respectively, compared to the experimental data at AGS, SPS, RHIC, and LHC, taken from papers [42, 80–87]. The pp volumes are calculated as a product $R_{\text{out}}R_{\text{side}}R_{\text{long}}$ of respective experimental radii. The blue lines correspond to pure HKM results, whereas the quantum corrections to them are presented by the red lines. Figure is taken from [40].

formation are under discussion. Therefore, for successful and unambiguous application of the correlation femtoscopy method to the case of elementary particle collisions, one needs to know the mechanisms of nonfemtoscopic correlations to separate the femtoscopic and nonfemtoscopic ones.

The two-particle correlation function is defined as

$$C(p_1, p_2) = \frac{P(p_1, p_2)}{P(p_1)P(p_2)}, \quad (31)$$

where $P(p_1, p_2)$ is the probability of observing two particles with momenta \mathbf{p}_1 and \mathbf{p}_2 , while $P(p_1)$ and $P(p_2)$ designate the single-particle probabilities. In heavy ion collisions

$$C(p_1, p_2) \approx C_F(\mathbf{p}, \mathbf{q}), \quad (32)$$

where $\mathbf{p} = (\mathbf{p}_1 + \mathbf{p}_2)/2$, $\mathbf{q} = \mathbf{p}_2 - \mathbf{p}_1$, and C_F denotes the femtoscopic correlation function that takes into account quantum statistics and final state interactions. In elementary particle collisions additional (nonfemtoscopic) correlations, like those arising from jet/string fragmentation and from energy and momentum conservation (see, e.g., [41–43]), can also give a significant contribution. The important problem

in this regard is whether we can factorize out the part corresponding to the nonfemtoscopic correlations, C_{NF} , from the total correlation function:

$$C(p_1, p_2) = C_F(\mathbf{p}, \mathbf{q})C_{NF}(\mathbf{p}, \mathbf{q}). \quad (33)$$

It [39], such a factorization, was demonstrated numerically within the simple models of three- and two-particle emission accounting for minijets fragmentation and event-by-event initial state fluctuation induced nonfemtoscopic correlations, and below we will assume this factorization property.

Recently, the ALICE Collaboration utilized some event generators, which do not include effects of quantum statistics, for an estimate of the correlation baseline (i.e., nonfemtoscopic correlation function of identical pions) under the Bose-Einstein peak at LHC energies [41, 42]. It was motivated by a reasonable agreement of the corresponding event generator simulations with the experimental data for correlation functions of oppositely charged pions in $p + p$ collisions at the same energy [41, 42]. The calculated correlation baseline has been utilized by the ALICE Collaboration to extract femtoscopic correlations from measured identical pion two-particle correlation functions [41]. Because the utilized event generators account for energy-momentum conservation and emission of minijets, it was conjectured in [41, 42] that some specific peculiarities of the unlike-sign pion correlations as well as like-sign nonfemtoscopic pion correlations can be caused by the jet-like and energy-momentum conservation induced correlations. In [46], we support this conjecture. There, to describe the nonfemtoscopic pion correlations in a simple analytical model, we assume that N pions are produced with momenta $\mathbf{p}_1, \dots, \mathbf{p}_N$ in $(N + X)$ multiparticle production events and consider pions as distinguishable, yet equivalent particles with symmetrical probability density functions. A distinguishability of equivalent particles means that there is no quantum interference between possibilities that correspond to all $N!$ permutations of the particle momenta p_i . Then single-particle probability, $P_N(p_1)$, and the two-particle probability, $P_N(p_1, p_2)$, can be written as

$$P_N(p_1) = \frac{1}{N} \sum_{i=1}^N \int d\Omega_{p^*} E_i^* \delta^{(3)}(\mathbf{p}_1 - \mathbf{p}_i^*) \hat{P}_N(p_1^*, \dots, p_N^*), \quad (34)$$

$$\begin{aligned} P_N(p_1, p_2) &= \frac{1}{N(N-1)} \sum_{i \neq j=1}^N \int d\Omega_{p^*} E_i^* \delta^{(3)}(\mathbf{p}_1 - \mathbf{p}_i^*) E_j^* \\ &\quad \times \delta^{(3)}(\mathbf{p}_2 - \mathbf{p}_j^*) \hat{P}_N(p_1^*, \dots, p_N^*), \end{aligned} \quad (35)$$

where $d\Omega_p = (d^3 p_1)/E_1 \cdots (d^3 p_N)/E_N$. The nonsymmetrized N -pion probability density in such events reads as

$$\begin{aligned} \widehat{P}_N(p_1, \dots, p_N) \\ = \frac{1}{K} \sum_X \int d\Omega_k \delta^{(4)} \left(p_a + p_b - \sum_{i=1}^N p_i - \sum_{j=1}^X k_j \right) \\ \times |M_{N+X}(p_1, \dots, k_X)|^2, \end{aligned} \quad (36)$$

where $M_{N+X}(p_1, \dots, k_X)$ is nonsymmetrized $(N+X)$ -particle production amplitude, p_a and p_b are 4-momenta of colliding particles (protons), and K is the normalization factor,

$$\begin{aligned} K = \sum_X \int d\Omega_k d\Omega_p \delta^{(4)} \left(p_a + p_b - \sum_{i=1}^N p_i - \sum_{j=1}^X k_j \right) \\ \times |M_{N+X}(p_1, \dots, k_X)|^2. \end{aligned} \quad (37)$$

Expression (36) for $\widehat{P}_N(p_1, \dots, p_N)$ is rather complicated because, in particular, it depends on X particles that are produced in addition to N pions. The latter means also that one can hardly expect that total energy or momentum of the pion subsystems are constants in the system's center of mass; instead, one can expect that they fluctuate in event-by-event basis. Here we assume that the total transverse momentum of N pions is equal to zero in the system's center of mass (keeping, however, in mind that this constraint is, in fact, too strong and can be weakened if necessary) and neglect the constraints conditioned by the conservation of energy and longitudinal momentum supposing that the system under consideration is barely N -pion subsystem in a small midrapidity region of the total system. Then, motivated by (36), we assume that a nonsymmetrized N -pion probability density can be written as

$$\widehat{P}_N(p_1, \dots, p_N) = \frac{1}{K} \delta(p_1, \dots, p_N) F_N(p_1, \dots, p_N), \quad (38)$$

where $F_N(p_1, \dots, p_N)$ is a nonsymmetrized function of pionic momenta, $\delta(p_1, \dots, p_N)$ denotes average constraints on the N -pion states that appear due to energy and momentum conservations in multiparticle production events, and we assume that

$$\delta(p_1, \dots, p_N) = \delta^{(2)}(\mathbf{p}_{T1} + \mathbf{p}_{T2} + \cdots + \mathbf{p}_{TN}), \quad (39)$$

where $\mathbf{p}_{T1}, \mathbf{p}_{T2}, \dots, \mathbf{p}_{TN}$ are transverse components of the momenta of the N particles. Then the normalization factor is

$$K = \int d\Omega_p \delta(p_1, \dots, p_N) F_N(p_1, \dots, p_N). \quad (40)$$

Now, to describe the nonfemtoscopic pion correlations in a simple analytical model, we assume that there are no other correlations in the production of N -pion states except for the correlations induced by transverse momentum conservation and cluster (minijet) structures in momentum space. For the

sake of simplicity we assume here that the only two-particle clusters appear. Then one can write for fairly large $N \gg 1$

$$\begin{aligned} F_N(p_1, \dots, p_N) \\ = f(p_1) \cdots f(p_N) Q(p_1, p_2) \cdots Q(p_{N-1}, p_N), \end{aligned} \quad (41)$$

where $Q(p_i, p_j)$ denotes the jet-like correlations between momenta \mathbf{p}_i and \mathbf{p}_j ; existence of such correlations means that F_N cannot be expressed as a product of one-particle distributions. Then, utilizing the integral representation of the δ -function by means of the Fourier transformation, $\delta^{(2)}(\mathbf{p}_T) = (2\pi)^{-2} \int d^2 r_T \exp(i\mathbf{r}_T \mathbf{p}_T)$, and accounting for (34), (38), (39), and (41), the single-particle probability reads as

$$P_N(p_1) = \frac{1}{(2\pi)^2 K} \int d^2 r_T G_N(\mathbf{p}_1, \mathbf{r}_T), \quad (42)$$

where

$$\begin{aligned} G_N(\mathbf{p}_1, \mathbf{r}_T) = \int d\Omega_{p^*} E_1^* \delta^{(3)}(\mathbf{p}_1 - \mathbf{p}_1^*) \\ \times e^{i\mathbf{r}_T(\mathbf{p}_{T1}^* + \cdots + \mathbf{p}_{TN}^*)} \\ \times F_N(p_1^*, \dots, p_N^*). \end{aligned} \quad (43)$$

A possibility of different cluster configurations of particles means, in particular, that registered particles with momenta \mathbf{p}_1 and \mathbf{p}_2 can belong either to different minijets or to the same minijet. Then, taking into account (35), (38), (39), and (41), we get

$$\begin{aligned} P_N(p_1, p_2) = \frac{N}{N(N-1)} P_N^{1\text{jet}}(p_1, p_2) \\ + \frac{N(N-1) - N}{N(N-1)} P_N^{2\text{jet}}(p_1, p_2), \end{aligned} \quad (44)$$

where

$$P_N^{1\text{jet}}(p_1, p_2) = \frac{1}{(2\pi)^2 K} \int d^2 r_T G_N^{1\text{jet}}(\mathbf{p}_1, \mathbf{p}_2, \mathbf{r}_T), \quad (45)$$

$$P_N^{2\text{jet}}(p_1, p_2) = \frac{1}{(2\pi)^2 K} \int d^2 r_T G_N^{2\text{jet}}(\mathbf{p}_1, \mathbf{p}_2, \mathbf{r}_T), \quad (46)$$

$$\begin{aligned} G_N^{1\text{jet}}(\mathbf{p}_1, \mathbf{p}_2, \mathbf{r}_T) = \int d\Omega_{p^*} E_i^* \delta^{(3)}(\mathbf{p}_1 - \mathbf{p}_1^*) E_j^* \\ \times \delta^{(3)}(\mathbf{p}_2 - \mathbf{p}_2^*) e^{i\mathbf{r}_T(\mathbf{p}_{T1}^* + \cdots + \mathbf{p}_{TN}^*)} F_N, \end{aligned} \quad (47)$$

$$\begin{aligned} G_N^{2\text{jet}}(\mathbf{p}_1, \mathbf{p}_2, \mathbf{r}_T) = \int d\Omega_{p^*} E_i^* \delta^{(3)}(\mathbf{p}_1 - \mathbf{p}_1^*) E_j^* \\ \times \delta^{(3)}(\mathbf{p}_2 - \mathbf{p}_3^*) e^{i\mathbf{r}_T(\mathbf{p}_{T1}^* + \cdots + \mathbf{p}_{TN}^*)} F_N. \end{aligned} \quad (48)$$

Here $F_N \equiv F_N(p_1^*, \dots, p_N^*)$. The first term in the right hand side of (44) is associated with events where the two registered particles belong to the same minijet, and the second term

corresponds to events where the particles are from different minijets. Evidently, the former is relatively rare; however, notice that the first term can be significant for small systems with not very large N .

It was demonstrated in [46] that this model can reproduce, with reasonable parameters, the correlation functions of unlike-sign pions measured by the ALICE Collaboration [41] and nonfemtoscopic correlations of like-sign pions that are generated in the PHOJET simulations and utilized as the correlation baseline by the ALICE Collaboration [41]. To calculate nonfemtoscopic correlations, analytical parameterizations of the functions in interest were used, namely,

$$f(p_i) = E_i \exp\left(-\frac{\mathbf{p}_{i,T}^2}{T_T^2}\right) \exp\left(-\frac{\mathbf{p}_{i,L}^2}{T_L^2}\right), \quad (49)$$

$$Q(p_i, p_j) = \exp\left(-\frac{(\mathbf{p}_i - \mathbf{p}_j)^2}{\alpha^2}\right), \quad (50)$$

where T_T, T_L , and α are some parameters, and we assume that $T_L \gg T_T$. In accordance with ALICE baseline obtained from the PHOJET event generator simulations, we assume that only $q_{\text{inv}} = \sqrt{(\mathbf{p}_2 - \mathbf{p}_1)^2 - (E_2 - E_1)^2}$ is measured for each \mathbf{p}_T bin. Assuming that longitudinal components of the registered particles are equal to zero, $p_{1L} = p_{2L} = 0$, we approximate q_{inv}^2 as

$$q_{\text{inv}}^2 \approx \mathbf{q}_T^2 \left(\frac{m^2 + \mathbf{p}_T^2 \sin^2 \phi}{m^2 + \mathbf{p}_T^2} \right), \quad (51)$$

where ϕ denotes unregistered angle between \mathbf{p}_T and \mathbf{q}_T , $\mathbf{p}_T \mathbf{q}_T = |\mathbf{p}_T| |\mathbf{q}_T| \cos \phi$. Then

$$C_{NF}(|\mathbf{p}_T|, q_{\text{inv}}) = \frac{\int_0^{2\pi} d\phi P_N(p_1, p_2)}{\int_0^{2\pi} d\phi P_N(p_1) P_N(p_2)}, \quad (52)$$

and, taking into account (44), we get

$$C_{NF}(|\mathbf{p}_T|, q_{\text{inv}}) = \frac{N-2}{N-1} \times \left(C_M^{2\text{jet}}(|\mathbf{p}_T|, q_{\text{inv}}) + \frac{1}{N-2} C_N^{1\text{jet}}(|\mathbf{p}_T|, q_{\text{inv}}) \right), \quad (53)$$

where

$$C_N^{2\text{jet}}(|\mathbf{p}_T|, q_{\text{inv}}) = \frac{\int_0^{2\pi} d\phi P_N^{2\text{jet}}(p_1, p_2)}{\int_0^{2\pi} d\phi P_N(p_1) P_N(p_2)}, \quad (54)$$

$$C_N^{1\text{jet}}(|\mathbf{p}_T|, q_{\text{inv}}) = \frac{\int_0^{2\pi} d\phi P_N^{1\text{jet}}(p_1, p_2)}{\int_0^{2\pi} d\phi P_N(p_1) P_N(p_2)}. \quad (55)$$

It is well known (see, e.g., [44, 45]) that the influence of exact conservation laws on single-particle and two-particle momentum probability densities at the N -particle production process depends on the value of N and disappears

at $N \rightarrow \infty$. Since one considers a subsystem of N pions but not the total system, to weaken the influence of the total transverse momentum conservation on pions we will consider $C_M^{1\text{jet}}$ and $C_M^{2\text{jet}}$ with $M > N$ instead of $C_N^{1\text{jet}}$ and $C_N^{2\text{jet}}$ in (53). This is the simplest way to account for a weakened conservation law in our model. At the same time, the factor $1/(N-2)$ in (53) remains the same since it is associated with the combinatorics of the distribution of particles between clusters in momentum space (“minijets”), which happens whether or not one weakens the total momentum conservation law. Also, for more exact fitting of the data points in each average transverse momentum bin, we utilize the auxiliary factors Λ ; when we compared results of our calculations with ALICE two-pion correlation and simulation data, these proportionality factors differ slightly from unit in our calculations (nearly 0.9). Then (53) gets the form

$$C_{NF}(|\mathbf{p}_T|, q_{\text{inv}}) = \Lambda(|\mathbf{p}_T|) \times \left(C_M^{2\text{jet}}(|\mathbf{p}_T|, q_{\text{inv}}) + \frac{1}{N-2} C_M^{1\text{jet}}(|\mathbf{p}_T|, q_{\text{inv}}) \right). \quad (56)$$

The results of our calculations of the nonfemtoscopic correlation functions C_{NF} are shown in Figures 8 and 9 in comparison with correlation functions reported by the ALICE Collaboration [41] for different transverse momenta of pion pairs (actually, we performed calculations for the mean value in each bin). The data for unlike-sign pion correlations measured by the ALICE Collaboration as well as for the PHOJET simulations of like-sign two-pion nonfemtoscopic correlation functions at midrapidity for the total charged multiplicity $N_{\text{ch}} \geq 12$ bin in $p+p$ collisions at $\sqrt{s} = 900$ GeV are taken from [41, 95]. Note that correlations of nonidentical pions measured by the ALICE Collaboration, as well as the PHOJET simulations of identical two-pion correlation functions, demonstrate Coulomb FSI correlations at the lowest q_{inv} bin and peaks coming from resonance decays. These Coulomb FSI and contributions from resonance production are not taken into account and so are not reproduced in our model. The presented results are obtained for $M = 50$, $T_T = \alpha = 0.65$ GeV (to minimize the number of fit parameters, we fixed $T_T = \alpha$ for all calculations. Note that with these parameter values the mean transverse momentum $\langle p_T \rangle$ is about 0.58 GeV), and the fitted values of N are different for like-sign and unlike-sign pion pairs, namely, $N^{\pm\pm} = 20$ for the former and $N^{+-} = 11$ for the latter. The relatively high value of M can be interpreted as a residual effect on the pion subsystem of total energy-momentum conservation in a multiparticle production process. The relation $N^{+-} < N^{\pm\pm}$ between fitted N values means that the magnitude of the correlations induced by a minijet for unlike-sign pion pairs is higher than that for like-sign ones. This happens because in the former there is no local charge conservation constraint for the production of oppositely charged pion pairs, and, therefore, one can expect less identically charged pion pairs from the fragmenting minijets than oppositely charged ones. One can

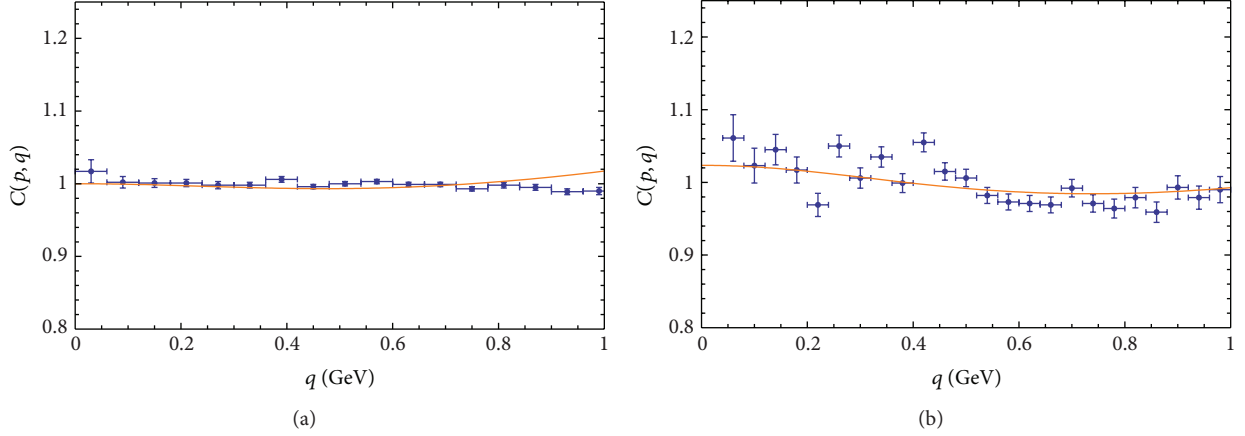


FIGURE 8: The nonfemtoscopic correlation functions of like-sign (a) and unlike-sign (b) pions in the $0.1 < p_T < 0.25$ GeV bin from a simulation using PHOJET [41, 95] (solid dots) and those calculated from the analytical model: minijets + momentum conservation (solid line). See the text for details.

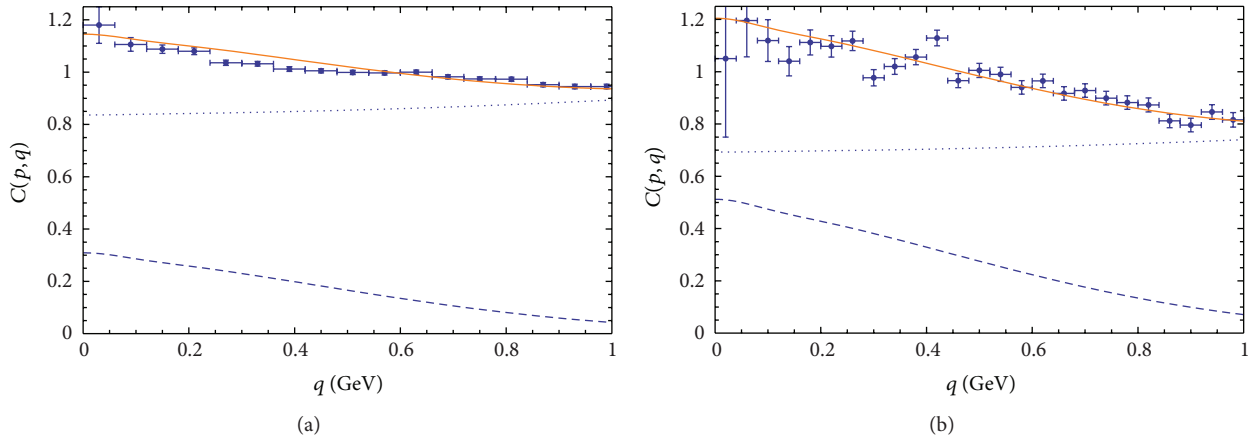


FIGURE 9: The nonfemtoscopic correlation functions of like-sign pions (a) from a simulation using PHOJET and unlike-sign pions (b) measured by the ALICE Collaboration in the $0.7 < p_T < 1.0$ GeV bin from [41, 95] (solid dots) and those calculated from the analytical model (solid line). The contributions to the nonfemtoscopic correlation function from the first term of (56) (dotted line) and from the second one (dashed line) are also presented.

see from the figures that the behavior of the nonfemtoscopic correlation functions of pions, C_{NF} , is reproduced well despite the simplicity of our model. This is a result of the competition of the two trends: an increase of the correlation function with q_{inv} because of momentum conservation and its decrease due to fragmentation of one minijet into the registered pion pair. Figure 9 also demonstrates the relative contribution of the first and second terms in (56) to the nonfemtoscopic correlation functions.

Another type of correlations not induced by the QS effects is the correlations connected with existence of subensembles of events with different emission functions that leads to the corresponding fluctuations in single-particle and two-particle momentum spectra. In hydrodynamical models of nucleus-nucleus and proton-proton collisions these fluctuations can be caused by asymmetrically fluctuating initial densities used for the hydrostage of the model. Let us consider the effect of such correlations on the resulting correlation

function on the example of a simple analytical model [46]. Disregarding the QS correlations (for model of two-particle emission that accounts for the QS see [39]) we suppose that the N -particle probability density is defined as

$$P_N(p_1, p_2, \dots, p_N) = \sum_i w(u_i) P_N(p_1, p_2, \dots, p_N; u_i), \quad (57)$$

where $P_N(p_1, p_2, \dots, p_N; u_i)$ is the N -particle probability density for some u_i type of the initial conditions, and $w(u_i)$ denotes the distribution over initial conditions, $\sum_i w(u_i) = 1$. To analyze the possible effect of fluctuating initial conditions, here we neglect conservation law constraints and the production of minijets. Because we assume uncorrelated particle emissions for each specific initial condition, one can write

$$\begin{aligned} P_N(p_1, p_2, \dots, p_N; u_i) \\ = f(p_1; u_i) f(p_2; u_i) \cdots f(p_{N-1}; u_i) f(p_N; u_i), \end{aligned} \quad (58)$$

where we normalize $f(p; u_i)$ as $\int (d^3 p/E) f(p; u_i) = 1$, and then $K = 1$; see (38) and (40). The two-particle nonfemtoscopic correlation function C_{NF} then reads as

$$C_{NF}(p_1, p_2) = \frac{\sum_i w(u_i) f(p_1; u_i) f(p_2; u_i)}{\sum_i w(u_i) f(p_1; u_i) \sum_j w(u_j) f(p_2; u_j)}. \quad (59)$$

Evidently, the different type of fluctuation, that is, the form of the distribution $w(u_i)$, leads to a different behavior of the nonfemtoscopic correlations. To illustrate that fluctuations can lead to the nonfemtoscopic correlation functions that are similar to the ones induced by minijets, let us consider the toy model where

$$w(\mathbf{u}_T) = \frac{\alpha^2}{\pi} \exp(-\mathbf{u}_T^2 \alpha^2), \quad (60)$$

$$f(p; \mathbf{u}_T) = \frac{\beta^2 \gamma}{\pi^{3/2}} E \exp(-(\mathbf{p}_T - \mathbf{u}_T)^2 \beta^2) \exp(-p_L^2 \gamma^2), \quad (61)$$

and normalization is chosen in such a way that $\int d^2 u_T w(\mathbf{u}_T) = 1$ and $\int (d^3 p/E) f(p; \mathbf{u}_T) = 1$. The main feature of such a model is that event-by-event single-particle transverse momentum spectra have a maximum for event-by-event fluctuating \mathbf{p}_T values. Such momentum spectrum fluctuations could take place, for example, in hydrodynamics with a highly inhomogeneous initial energy density profile without cylindrical or elliptic symmetry. One can easily see that in this case C_{NF} decreases with q_T^2 ,

$$C_{NF}(p, q) \sim \exp\left(-\frac{\beta^4}{2(\alpha^2 + \beta^2)} q_T^2\right), \quad (62)$$

and this means (after taking into account (51) and (52)) that C_{NF} decreases with q_{inv}^2 too, which is similar to the behavior of C_{NF} if the nonfemtoscopic correlations are induced by minijets. At the same time, unlike the latter, the hydrodynamical fluctuations lead to similar correlations for like-sign and unlike-sign pion pairs. Then, our analysis suggests that, up to different resonance yields, the value of the slope of the correlation baseline at relatively low q_{inv} can be somewhere between pure hydrodynamic (i.e., the same as for nonidentical pion pairs) and pure minijet (i.e., lower than for nonidentical pion pairs) scenarios.

7. Summary

It is often said that the femtoscopic measurements allow one to restore the space-time structure of the particle/nucleus collision processes. It is really possible but only through the theoretical constructions allowing to interpret these processes and describe the wide range of the corresponding experimental data. If such an advanced model is based on some kind of the space-time picture, then the crucial point for the model is a recreation of the femtoscopic data. If it is successful, then, first, this model claims to be true, and,

second, the same is related to recover by the model the space-time structure of a collision process.

In this review we analyzed hydrokinetic model (HKM) for $A + A$ collisions as the reliable theoretical construction for description of the momentum spectra of pions, kaons, protons/antiprotons, all charged particles, and elliptic flows, in wide range of different centralities [29, 30] at RHIC and LHC. We demonstrate here that it describes well the available femtoscopic data for $Au + Au$ and $Pb + Pb$ collisions.

A particular interest is the theoretical basis of HKM which is grounded on the escape functions (not on the distribution ones) when the particle liberation process from the expanding medium is described within the Boltzmann equation. This allows one to avoid the principal problem of the particlization of a medium at nonspace-like sites of transition hypersurfaces, where medium evolution converts into hadronic cascade, like the UrQMD one. So, using the hydrokinetics, as the ‘‘buffer’’ zone, one can switch to hadronic cascade at some space-like hypersurface with a nonequilibrium particle input from HKM. In review we describe just this hybrid variant of the HKM + UrQMD (hHKM).

The HKM, UrQMD, and other existing models/event generators are quasiclassical constructions, and quantum elements, like Bose-Einstein correlations, are inputted typically at the very late stage as the external weights of the boson pair states. In its turn such a procedure is based on the model of independent chaotic sources [4–6]. It is found recently [39] that such a model is inadequate for fairly small sources where the uncertainty principle leads to (partial) indistinguishability of closely located emitters that fundamentally impedes their full independence and incoherence. We review the recent results as for the correlation femtoscopy method that is going beyond the standard approach of independent/random particle emission. The partial coherence of emitted particles is because of the quantum nature of particle emission and happens even if there is no specific mechanism to produce a coherent component of the source radiation. The measure of distinguishability/indistinguishability and mutual coherence of the two emitted wave packets is associated with their overlap integral. In thermal systems the role of corresponding coherent length is played by the thermal de Broglie wavelength.

The application of the new femtoscopy method is demonstrated using the results of [40], where it was found that quantum corrections to the pion interferometry radii in $p + p$ collisions at the LHC can significantly improve the (semiclassical) event generator results that typically give an overestimate of the experimental interferometry radii and volumes. The effects become important for small sources, 1–2 fm or smaller. Such systems cannot be completely random and so require the modification of the standard theoretical approach for the correlation femtoscopy.

More sophisticated result of this study is a good applicability of the hydrodynamics/hydrokinetics with the quantum corrections for description of the femtoscopy scales not only in $A + A$ collisions but also, at least for large multiplicities, in $p + p$ events. These scales are well reproduced for not

large p_T . Whether it means the validity of the hydrodynamic mechanism for the bulk matter production in the LHC $p + p$ collisions is still an open question. It is also related to the problem of early thermalization in the processes of heavy ion collisions; the nature of such phenomenon is still a fundamental theoretical issue.

For small systems the specific nonfemtoscopic correlations can appear in the same kinematic region as the femtoscopic ones. They could be a result of the cluster (minijet) structures in final momentum space of produced particles and the global energy-momentum conservation constraints. The latter typically result in an increase with q_{inv} for fairly high q_{inv} of the nonfemtoscopic two-pion correlation functions of small systems, whereas the former mostly determines a decrease of the ones at relatively low q_{inv} . We discuss the simple analytical model [46] that takes into account correlations induced by the total transverse momentum conservation as well as minijets and show that the model gives reasonable description of the two-pion nonfemtoscopic correlations of identical and nonidentical pions in proton-proton collision events at $\sqrt{s} = 900$ GeV reported by the ALICE Collaboration [41]. The important issue is that femtoscopic and nonfemtoscopic correlations are factorized [39].

There can be different types of multiparticle production mechanisms in $p + p$ collisions, and some of them could result in qualitatively similar nonfemtoscopic correlation functions. We discuss heuristic arguments [46] that the two-pion nonfemtoscopic correlation functions calculated in hydrodynamics with event-by-event fluctuating initial conditions can be qualitatively similar at relatively low q_{inv} to the ones calculated in the PHOJET-like generators, where the nonfemtoscopic correlations for low q_{inv} are mainly caused by minijets. It is worth noting an important difference between the nonfemtoscopic correlations induced by minijets and hydrodynamical fluctuations: while the former leads to a higher magnitude of the nonfemtoscopic correlations for unlike-sign pion pairs as compared to like-sign pions, the latter results in a similar (up to the resonance contributions) strength of the nonfemtoscopic correlations for identical and nonidentical pions. Then, if the applicability of hydrodynamics to $p + p$ collisions will be justified, such an analysis allows one to estimate the correlation baseline and, so, to extract the femtoscopic scales in these collisions by means of tuning the hydrokinetic model to reproduce the experimental unlike-sign pion correlations.

Acknowledgments

The research was carried out within the scope of the EUREA: European Ultra Relativistic Energies Agreement (European Research Group: "Heavy ions at ultrarelativistic energies") and is supported by the National Academy of Sciences of Ukraine (Agreement F4-2013) and by the State fund for Fundamental Researches of Ukraine (Agreement F33/24-2013). The work was supported by the Program of Fundamental Research of the Department of Physics and Astronomy of NAS Ukraine.

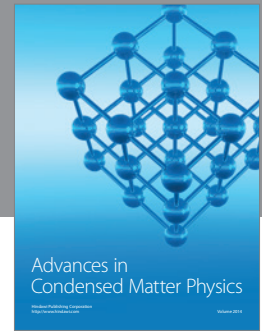
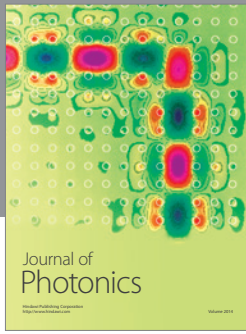
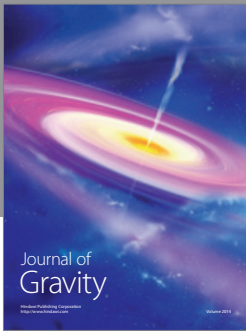
References

- [1] M. A. Lisa, S. Pratt, R. Soltz, and U. Wiedemann, "Femtосcopy in relativistic heavy ion collisions: two decades of progress," *Annual Review of Nuclear and Particle Science*, vol. 55, pp. 357–402, 2005.
- [2] M. Lisa and S. Pratt, "Femtoscopically probing the freeze-out configuration in heavy ion collisions," in *The Final Expansion State of Relativistic Nuclear Collisions*, R. Stock, Ed., vol. 23 of *Relativistic Heavy Ion Physics*, pp. 653–685, 2010.
- [3] Z. Chajęcki, "Femtосcopy in hadron and lepton collisions: world systematics," *Acta Physica Polonica B*, vol. 40, no. 4, pp. 1119–1136, 2009.
- [4] G. I. Kopylov and M. I. Podgoretsky, "Correlations of identical particles emitted by highly excited nuclei," *Soviet Journal of Nuclear Physics*, vol. 15, p. 219, 1972.
- [5] G. I. Kopylov and M. I. Podgoretsky, "Multiple production and interference of particles emitted by moving sources," *Soviet Journal of Nuclear Physics*, vol. 18, p. 336, 1974.
- [6] G. I. Kopylov and M. I. Podgoretsky, "Mutual coherence functions of elementary particles and multiple production," *Soviet Journal of Nuclear Physics*, vol. 19, p. 215, 1974.
- [7] G. Cocconi, "Second-order interference as a tool for the determination of hadron fireball dimensions," *Physics Letters B*, vol. 49, no. 5, pp. 459–461, 1974.
- [8] S. Pratt, "Pion interferometry for exploding sources," *Physical Review Letters*, vol. 53, no. 13, pp. 1219–1221, 1984.
- [9] S. Pratt, "Pion interferometry of quark-gluon plasma," *Physical Review D*, vol. 33, no. 5, pp. 1314–1327, 1986.
- [10] A. N. Makhlin and Yu. M. Sinyukov, "The pion interferometry theory for the hydrodynamic stage of multiple processes," *Soviet Journal of Nuclear Physics*, vol. 46, p. 345, 1987.
- [11] V. A. Averchenkov, A. N. Makhlin, and Yu. M. Sinyukov, "Study of collective motion in hadronic matter by a pion interferometry method," *Soviet Journal of Nuclear Physics*, vol. 46, p. 905, 1987.
- [12] A. N. Makhlin and Yu. M. Sinyukov, "The hydrodynamics of hadron matter under a pion interferometric microscope," *Zeitschrift für Physik C*, vol. 39, no. 1, pp. 69–73, 1988.
- [13] Yu. M. Sinyukov, "Hanbury Brown/Twiss correlations for expanding hadron and quark-gluon matter," *Nuclear Physics A*, vol. 498, no. C, pp. 151–159, 1989.
- [14] Y. Hama and S. S. Padula, "Bose-Einstein correlation of particles produced by expanding sources," *Physical Review D*, vol. 37, no. 11, pp. 3237–3245, 1988.
- [15] Yu. M. Sinyukov, "Spectra and correlations in locally equilibrium hadron and quark-gluon systems," *Nuclear Physics A*, vol. 566, no. C, pp. 589–592, 1994.
- [16] Yu. M. Sinyukov, "Boson spectra and correlations in small thermalized systems," in *Hot Hadronic Matter: Theory and Experiment*, J. Letessier, H. H. Gutbrod, and J. Rafelski, Eds., pp. 309–322, Plenum, New York, NY, USA, 1995.
- [17] S. V. Akkelin and Yu. M. Sinyukov, "The HBT-interferometry of expanding sources," *Physics Letters B*, vol. 356, no. 4, pp. 525–530, 1995.
- [18] S. V. Akkelin and Yu. M. Sinyukov, "The HBT-interferometry of expanding inhomogeneous sources," *Zeitschrift für Physik C*, vol. 72, no. 3, pp. 501–507, 1996.
- [19] U. Heinz, "The quark-gluon plasma at RHIC," *Nuclear Physics A*, vol. 721, pp. C30–C39, 2003.
- [20] S. Pratt, "Correlations and fluctuations, a summary of Quark Matter 2002," *Nuclear Physics A*, vol. 715, pp. 389c–398c, 2003.

- [21] S. Soff, S. A. Bass, D. H. Hardtke, and S. Y. Panitkin, “Particle correlations at RHIC—scrutiny of a puzzle,” *Nuclear Physics A*, vol. 715, pp. 801c–804c, 2003.
- [22] Yu. M. Sinyukov, “Matter evolution and soft physics in $A + A$ collisions,” *Acta Physica Polonica B*, vol. 37, no. 12, pp. 3343–3369, 2006.
- [23] S. V. Akkelin, Y. Hama, Iu. A. Karpenko, and Yu. M. Sinyukov, “Hydro-kinetic approach to relativistic heavy ion collisions,” *Physical Review C*, vol. 78, no. 3, Article ID 034906, 2008.
- [24] Yu. M. Sinyukov, A. V. Nazarenko, and Iu. A. Karpenko, “Is early thermalization really needed in $A + A$ collisions?” *Acta Physica Polonica B*, vol. 40, no. 4, pp. 1109–1117, 2009.
- [25] M. Gyulassy, Iu. Karpenko, A. V. Nazarenko, and Yu. M. Sinyukov, “HBT and initial conditions for hydrodynamic expansion in $A + A$ collisions,” *Brazilian Journal of Physics*, vol. 37, no. 3A, pp. 1031–1038, 2007.
- [26] W. Broniowski, W. Florkowski, M. Chojnacki, and A. Kisiel, “Free-streaming approximation in early dynamics of relativistic heavy-ion collisions,” *Physical Review C*, vol. 80, no. 3, Article ID 034902, 2009.
- [27] S. Pratt, “The long slow death of the HBT puzzle,” *Nuclear Physics A*, vol. 830, no. 1–4, pp. 51c–57c, 2009.
- [28] Iu. A. Karpenko and Yu. M. Sinyukov, “Energy dependence of pion interferometry scales in ultra-relativistic heavy ion collisions,” *Physics Letters B*, vol. 688, no. 1, pp. 50–54, 2010.
- [29] Iu. A. Karpenko and Yu. M. Sinyukov, “Kaon and pion femtoscopy at the highest energies available at the BNL Relativistic Heavy Ion Collider (RHIC) in a hydrokinetic model,” *Physical Review C*, vol. 81, no. 5, Article ID 054903, 2010.
- [30] Iu. A. Karpenko, Yu. M. Sinyukov, and K. Werner, “description of bulk observables in the hydrokinetic model of $A+A$ collisions at the BNL Relativistic Heavy Ion Collider and the CERN Large Hadron Collider,” *Physical Review C*, vol. 87, Article ID 024914, 2013.
- [31] K. Aamodt, B. Abelev, A. A. Quintana et al., “Elliptic flow of charged particles in Pb-Pb collisions at $\sqrt{s_{NN}} = 2.76$ TeV,” *Physical Review Letters*, vol. 105, Article ID 252302, 11 pages, 2010.
- [32] N. Armesto, N. Borghini, S. Jeon et al., Eds., “Heavy-ion collisions at the LHC—last call for predictions,” *Journal of Physics G*, vol. 35, no. 5, Article ID 054001, 2008.
- [33] K. Aamodt, A. A. Quintana, D. Adamová et al., “Two-pion Bose-Einstein correlations in central Pb-Pb collisions at $\sqrt{s_{NN}} = 2.76$ TeV,” *Physics Letters B*, vol. 696, no. 4, pp. 328–337, 2011.
- [34] M. Chojnacki, W. Florkowski, W. Broniowski, and A. Kisiel, “Soft heavy-ion physics from hydrodynamics with statistical hadronization: Predictions for collisions at $\sqrt{s_{NN}} = 5.5$ TeV,” *Physical Review C*, vol. 78, no. 1, Article ID 014905, 13 pages, 2008.
- [35] Yu. M. Sinyukov, S. V. Akkelin, and Y. Hama, “Freeze-out problem in hydrokinetic approach to $A + A$ collisions,” *Physical Review Letters*, vol. 89, no. 5, pp. 052301/1–052301/4, 2002.
- [36] Iu. A. Karpenko and Yu. M. Sinyukov, “Femtoscopic scales in central $A + A$ collisions at RHIC and LHC energies in a hydrokinetic model,” *Journal of Physics G*, vol. 38, no. 12, Article ID 124059, 2011.
- [37] S. A. Bass, M. Belkacem, M. Bleicher et al., “Microscopic models for ultrarelativistic heavy ion collisions,” *Progress in Particle and Nuclear Physics*, vol. 41, pp. 255–369, 1998.
- [38] M. Bleicher, E. Zabrodin, C. Spieles et al., “Relativistic hadron-hadron collisions in the ultra-relativistic quantum molecular dynamics model,” *Journal of Physics G*, vol. 25, no. 9, Article ID 1859, 1999.
- [39] Yu. M. Sinyukov and V. M. Shapoval, “Correlation femtoscopy of small systems,” *Physical Review D*, vol. 87, no. 9, Article ID 094024, 15 pages, 2013.
- [40] V. M. Shapoval, P. Braun-Munzinger, Iu. A. Karpenko, and Yu. M. Sinyukov, “Femtoscopic scales in $p + p$ and $p + Pb$ collisions in view of the uncertainty principle,” *Physics Letters B*, vol. 725, no. 1–3, pp. 139–147, 2013.
- [41] K. Aamodt, N. Abel, U. Abeysekara et al., “Two-pion Bose-Einstein correlations in pp collisions at $\sqrt{s} = 900$ GeV,” *Physical Review D*, vol. 82, no. 5, Article ID 052001, 14 pages, 2010.
- [42] K. Aamodt, A. A. Quintana, D. Adamová et al., “Femtoscopic of pp collisions at $\sqrt{s} = 0.9$ and 7 TeV at the LHC with two-pion Bose-Einstein correlations,” *Physical Review D*, vol. 84, no. 11, Article ID 112004, 22 pages, 2011.
- [43] M. M. Aggarwal, Z. Ahammed, A. V. Alakhverdyants et al., “Pion femtoscopy in $p + p$ collisions at $\sqrt{s} = 200$ GeV,” *Physical Review C*, vol. 83, Article ID 064905, 17 pages, 2011.
- [44] Z. Chajęcki and M. Lisa, “Global conservation laws and femtoscopy of small systems,” *Physical Review C*, vol. 78, no. 6, Article ID 064903, 2008.
- [45] Z. Chajęcki and M. Lisa, “Conservation laws and multiplicity evolution of spectra at energies available at the BNL Relativistic Heavy Ion Collider,” *Physical Review C*, vol. 79, no. 3, p. 034908, 2009.
- [46] S. V. Akkelin and Yu. M. Sinyukov, “Deciphering nonfemtoscopic two-pion correlations in $p + p$ collisions with simple analytical models,” *Physical Review D*, vol. 85, no. 7, Article ID 074023, 2012.
- [47] M. Janik, “ $\Delta\eta\Delta\phi$ angular correlations in pp collisions at the LHC registered by the ALICE experiment,” <http://arxiv.org/abs/1203.2844>.
- [48] F. Grassi, Y. Hama, and T. Kodama, “Continuous particle emission: a probe of thermalized matter evolution?” *Physics Letters B*, vol. 355, no. 1–2, pp. 9–14, 1995.
- [49] F. Grassi, Y. Hama, and T. Kodama, “Particle emission in the hydrodynamical description of relativistic nuclear collisions,” *Zeitschrift für Physik C*, vol. 73, pp. 153–160, 1996.
- [50] K. A. Bugaev, “Shock-like freeze-out in relativistic hydrodynamics,” *Nuclear Physics A*, vol. 606, no. 3–4, pp. 559–567, 1996.
- [51] F. Cooper and G. Frye, “Single-particle distribution in the hydrodynamic and statistical thermodynamic models of multiparticle production,” *Physical Review D*, vol. 10, no. 1, pp. 186–189, 1974.
- [52] Yu. M. Sinyukov, “Direct conversion of mixed phase into free hadronic gas and transverse pion momenta in ultra-relativistic nuclear collisions,” *Zeitschrift für Physik C*, vol. 43, pp. 401–409, 1989.
- [53] N. S. Amelin, R. Lednicky, T. A. Pocheptsov et al., “Fast hadron freeze-out generator,” *Physical Review C*, vol. 74, no. 6, Article ID 064901, 2006.
- [54] P. Huovinen and H. Petersen, “Particlization in hybrid models,” *The European Physical Journal A*, vol. 48, article 171, 2012.
- [55] M. Laine and Y. Schroder, “Quark mass thresholds in QCD thermodynamics,” *Physical Review D*, vol. 73, Article ID 085009, 13 pages, 2006.
- [56] K. Nakamura, J. Beringer, J.-F. Arguin et al., “Review of particle physics,” *Journal of Physics G*, vol. 37, Article ID 075021, 2010.

- [57] Yu. M. Sinyukov, R. Lednicky, S. V. Akkelin, J. Pluta, and B. Erazmus, "Coulomb corrections for interferometry analysis of expanding hadron systems," *Physics Letters B*, vol. 432, no. 3-4, pp. 248–257, 1998.
- [58] G. Goldhaber, S. Goldhaber, W. Lee, and A. Pais, "Influence of Bose-Einstein statistics on the antiproton-proton annihilation process," *Physical Review*, vol. 120, no. 1, pp. 300–312, 1960.
- [59] S. Pratt, "Validity of the smoothness assumption for calculating two-boson correlations in high-energy collisions," *Physical Review C*, vol. 56, no. 2, pp. 1095–1098, 1997.
- [60] A. Kisiel, W. Florkowski, W. Broniowski, and J. Pluta, "Femtoscopy in hydrodynamics-inspired models with resonances," *Physical Review C*, vol. 73, no. 6, Article ID 064902, 2006.
- [61] "ROOT Data Analysis Framework," <http://root.cern.ch/drupal/>.
- [62] O. Utyuzh, G. Wilk, and Z. Włodarczyk, "Modeling Bose-Einstein correlations via elementary emitting cells," *Physical Review D*, vol. 75, no. 7, Article ID 074030, 2007.
- [63] G. A. Kozlov, O. V. Utyuzh, G. Wilk, and Z. Włodarczyk, "Some forgotten features of the Bose-Einstein correlations," *Physics of Atomic Nuclei*, vol. 71, no. 9, pp. 1502–1504, 2008.
- [64] Yu. M. Sinyukov, "Boson spectra and correlations for thermal locally equilibrium systems," *Acta Physica Hungarica Series A*, vol. 10, pp. 113–136, 1999.
- [65] Yu. M. Sinyukov and B. Lorstad, "On intensity interferometry at high multiplicities," *Zeitschrift für Physik C*, vol. 61, pp. 587–592, 1994.
- [66] Yu. M. Sinyukov, S. V. Akkelin, and R. Lednicky, "Thermodynamics of multi-boson phenomena," in *Proceedings of the 8th International Workshop on Multiparticle Production in Matrahaza*, T. Csorgo, S. Hegyi, G. Hwa et al., Eds., p. 66, World Scientific.
- [67] R. Lednicky, V. Lyuboshitz, K. Mikhailov, Yu. M. Sinyukov, A. Stavinsky, and B. Erazmus, "Multiboson effects in multiparticle production," *Physical Review C*, vol. 61, no. 3, pp. 349011–3490119, 2000.
- [68] S. V. Akkelin, R. Lednicky, and Yu. M. Sinyukov, "Correlation search for coherent pion emission in heavy ion collisions," *Physical Review C*, vol. 65, no. 6, pp. 649041–6490416, 2002.
- [69] STAR Collaboration, "Pion interferometry in $Au + Au$ collisions at $\sqrt{s_{NN}} = 200$ GeV," *Physical Review C*, vol. 71, no. 4, Article ID 044906, 21 pages, 2005.
- [70] S. S. Adler, S. Afanasiev, C. Aidala et al., "Bose-Einstein correlations of charged pion pairs in $Au + Au$ collisions at $\sqrt{s_{NN}} = 200$ GeV," *Physical Review Letters*, vol. 93, no. 15, Article ID 152302, 6 pages, 2004.
- [71] P. Bozek, "Flow and interferometry in $(3 + 1)$ -dimensional viscous hydrodynamics," *Physical Review C*, vol. 85, no. 3, Article ID 034901, 9 pages, 2012.
- [72] L. Adamczyk, J. K. Adkins, G. Agakishiev et al., "Freeze-out dynamics via charged kaon femtoscopy in $\sqrt{s_{NN}} = 200$ GeV central $Au + Au$ collisions," <http://arxiv.org/abs/1302.3168>.
- [73] S. Afanasiev, C. Aidala, N. N. Ajitanand et al., "Charged kaon interferometric probes of space-time evolution in $Au + Au$ collisions at $\sqrt{s_{NN}} = 200$ GeV," *Physical Review Letters*, vol. 103, no. 14, Article ID 142301, 6 pages, 2009.
- [74] R. Lednicky, V. L. Lyuboshitz, and M. I. Podgoretsky, "Interference correlations of identical particles in models with closely spaced sources," *Yad. Fiz.*, vol. 38, p. 251, 1983, *Soviet Journal of Nuclear Physics*, vol. 38, pp. 147, 1983.
- [75] M. S. Nilsson, L. V. Bravina, E. E. Zabrodin, L. V. Malinina, and J. Bleibel, "Study of $\pi\pi$ correlations at LHC and RHIC energies in pp collisions within the quark-gluon string model," *Physical Review D*, vol. 84, no. 5, Article ID 054006, 2011.
- [76] E. K. G. Sarkisyan and A. S. Sakharov, "Relating multihadron production in hadronic and nuclear collisions," *The European Physical Journal C*, vol. 70, no. 3, pp. 533–541, 2010.
- [77] E. K. G. Sarkisyan and A. S. Sakharov, "Multihadron production features in different reactions," *AIP Conference Proceedings*, vol. 828, pp. 35–41, 2006.
- [78] B. Kopeliovich, A. Schäfer, and A. Tarasov, "Nonperturbative effects in gluon radiation and photoproduction of quark pairs," *Physical Review D*, vol. 62, no. 5, Article ID 054022, pp. 1–31, 2000.
- [79] E. V. Shuryak and I. Zahed, "Understanding nonperturbative deep-inelastic scattering: instanton-induced inelastic dipole-dipole cross section," *Physical Review D*, vol. 69, no. 1, Article ID 014011, 2004.
- [80] K. Aamodt, A. A. Quintanab, D. Adamová et al., "Two-pion Bose-Einstein correlations in central Pb-Pb collisions at $\sqrt{s_{NN}} = 2.76$ TeV," *Physics Letters B*, vol. 696, no. 4, pp. 328–337, 2011.
- [81] D. Antończyk, "Two pion correlations at SPS energies," *Acta Physica Polonica B*, vol. 40, no. 4, pp. 1137–1144, 2009.
- [82] S. V. Afanasiev, T. Anticic, D. Barna et al., "Energy dependence of pion and kaon production in central $Pb + Pb$ collisions," *Physical Review C*, vol. 66, no. 5, Article ID 054902, 9 pages, 2002.
- [83] C. Alt, T. Anticic, B. Baatar et al., "Bose-Einstein correlations of $\pi-\pi$ pairs in central $Pb + Pb$ collisions at 20A,30A,40A,80A, and 158A GeV," *Physical Review C*, vol. 77, no. 6, Article ID 064908, 20 pages, 2008.
- [84] J. Adams, C. Adler, M. M. Aggarwal et al., "Identified particle distributions in pp and $Au + Au$ collisions at $\sqrt{s_{NN}} = 200$ GeV," *Physical Review Letters*, vol. 92, no. 11, Article ID 112301, 6 pages, 2004.
- [85] J. Adams, M. M. Aggarwal, Z. Ahammed et al., "Pion interferometry in $Au + Au$ collisions at $\sqrt{s_{NN}} = 200$ GeV," *Physical Review C*, vol. 71, no. 4, Article ID 044906, 21 pages, 2004.
- [86] S. S. Adler, S. Afanasiev, C. Aidala et al., "Identified charged particle spectra and yields in $Au + Au$ collisions at $\sqrt{s_{NN}} = 200$ GeV," *Physical Review C*, vol. 69, no. 3, Article ID 034909, 32 pages, 2004.
- [87] S. S. Adler, S. Afanasiev, C. Aidala et al., "Bose-Einstein correlations of charged pion pairs in $Au + Au$ collisions at $\sqrt{s_{NN}} = 200$ GeV," *Physical Review Letters*, vol. 93, no. 15, Article ID 152302, 6 pages, 2004.
- [88] S. V. Akkelin and Yu. M. Sinyukov, "Phase-space densities and effects of resonance decays in a hydrodynamic approach to heavy ion collisions," *Physical Review C*, vol. 70, no. 6, Article ID 064901, 17 pages, 2004.
- [89] S. V. Akkelin and Yu. M. Sinyukov, "Hanbury-Brown-Twiss search for new states of matter in $A + A$ collisions," *Physical Review C*, vol. 73, no. 3, Article ID 034908, 2006.
- [90] T. Csorgo and B. Lorstad, "Bose-Einstein correlations for three-dimensionally expanding, cylindrically symmetric, finite systems," *Physical Review C*, vol. 54, no. 3, pp. 1390–1403, 1996.
- [91] S. V. Akkelin, P. Braun-Munzinger, and Yu. M. Sinyukov, "Reconstruction of hadronization stage in $Pb + Pb$ collisions at 158 A GeV/c," *Nuclear Physics A*, vol. 710, no. 3-4, pp. 439–465, 2002.
- [92] P. Csizmadia, T. Csorgo, and B. Lukacs, "New analytic solutions of the non-relativistic hydrodynamical equations," *Physics Letters B*, vol. 443, no. 1–4, pp. 21–25, 1998.

- [93] G. F. Bertsch, "Meson phase space density in heavy ion collisions from interferometry," *Physical Review Letters*, vol. 72, no. 15, pp. 2349–2350, 1994.
- [94] G. F. Bertsch, "Meson phase space density in heavy ion collisions from interferometry," *Physical Review Letters*, vol. 77, pp. 789–789, 1996.
- [95] "The Durham HepData Project," <http://hepdata.cedar.ac.uk/>.



Hindawi

Submit your manuscripts at
<http://www.hindawi.com>

